

Long-Range Rapidity Correlations in Heavy-Light Ion Collisions

Yuri V. Kovchegov,^a Douglas E. Wertepny^b

Department of Physics, The Ohio State University, Columbus, OH 43210, USA

We study two-particle long-range rapidity correlations arising in the early stages of heavy ion collisions in the saturation/Color Glass Condensate framework, assuming for simplicity that one colliding nucleus is much larger than the other. We calculate the two-gluon production cross section while including all-order saturation effects in the heavy nucleus with the lowest-order rescattering in the lighter nucleus. We find four types of correlations in the two-gluon production cross section: (i) geometric correlations, (ii) HBT correlations accompanied by a back-to-back maximum, (iii) away-side correlations, and (iv) near-side azimuthal correlations which are long-range in rapidity. The geometric correlations (i) are due to the fact that nucleons are correlated by simply being confined within the same nucleus and may lead to long-range rapidity correlations for the produced particles without strong azimuthal angle dependence. Somewhat surprisingly, long-range rapidity correlations (iii) and (iv) have exactly the same amplitudes along with azimuthal and rapidity shapes: one centered around $\Delta\phi = \pi$ with the other one centered around $\Delta\phi = 0$ (here $\Delta\phi$ is the azimuthal angle between the two produced gluons). We thus observe that the early-time CGC dynamics in nucleus-nucleus collisions generates azimuthal non-flow correlations which are qualitatively different from jet correlations by being long-range in rapidity. If strong enough, they have the potential of mimicking the elliptic (and higher-order even-harmonic) flow in the di-hadron correlators: one may need to take them into account in the experimental determination of the flow observables.

PACS numbers: 25.75.-q, 25.75.Gz, 12.38.Bx, 12.38.Cy

I. INTRODUCTION

Long-range rapidity correlations between pairs of hadrons produced at small azimuthal angles with respect to each other were discovered recently in heavy ion (AA) [1–4], proton–proton (pp) [5], and proton–nucleus (pA) collisions [6]. Due to the particular shape of the corresponding correlation function, with a narrow correlation in the azimuthal angle $\Delta\phi$ and a wide correlation in pseudo-rapidity separation $\Delta\eta$, these correlations are often referred to as the “ridge”.

There appears to be a consensus in the community that the origin of these long-range rapidity correlations is in the very early-time dynamics immediately following the collision. A simple causality argument demonstrates that a correlation between two hadrons produced far apart in rapidity may arise only in their common causal past, that is, in the early stages of the collision [7, 8]. However, the detailed dynamical origin of these “ridge” correlations is not completely clear.

It has been proposed in the literature [7–15] that the “ridge” correlations may arise in the classical gluon field dynamics of the parton saturation physics/Color Glass Condensate (CGC). (For reviews of saturation/CGC physics see [16–20].) Indeed classical gluon fields, which in the McLerran–Venugopalan (MV) model [21–23] dominate gluon production in heavy ion collisions, do lead to a rapidity-independent distribution of the produced gluons [24–27] over rapidity intervals of up to $\Delta y \lesssim 1/\alpha_s$, which is the upper limit of their validity (with α_s the strong coupling constant). Correlations between such classical fields, introduced in the process of averaging over their color sources, do have a long range in rapidity [7, 8, 28]. Moreover, it was observed in [7, 11–13] that the diagrams giving rise to such rapidity correlations also lead to a narrow correlation in the azimuthal direction, in qualitative agreement with the shape of the “ridge” correlation.

One has to keep in mind that in heavy ion collisions the early-stage azimuthal correlation may be washed out by the final state interactions leading to thermalization of the produced medium and its hydrodynamic evolution. (Note though, that the rapidity correlation is not likely to be strongly affected by such late-time dynamics.) It was argued, however, that the effect of the radial flow in the hydrodynamic evolution of the quark-gluon plasma (QGP) would be to (re-)introduce the azimuthal correlations [8].

Another potential complication with the CGC explanation of the “ridge” is the fact that rapidity-dependent corrections to classical gluon fields do become important at rapidity of the order of $\Delta y \sim 1/\alpha_s$. These corrections come in through the non-linear Balitsky–Kovchegov (BK) [29–32] and Jalilian-Marian–Iancu–McLerran–Weigert–Leonidov–Kovner (JIMWLK) [33–36] evolution equations. Rapidity-dependent corrections are very important for describing the

^a kovchegov.1@asc.ohio-state.edu

^b wertepny.1@osu.edu

hadron multiplicity distribution in rapidity, dN/dy , in the CGC framework [37]. As dN/dy does depend on rapidity rather strongly in RHIC heavy ion data, and also strongly (albeit less so) in the LHC data, it is very hard to describe without the rapidity-dependent nonlinear evolution. It is possible that similar rapidity-dependent corrections may significantly affect and potentially destroy the long-range structure of the rapidity correlations due to classical gluon fields of the MV model. Note that progress on this issue has been made in [11], indicating that inclusion of small- x evolution still leaves the “ridge” reasonably flat in rapidity until $\Delta y \sim 1/\alpha_s$ when the correlation disappears.

To elucidate the above questions and concerns, and to improve the precision of the CGC predictions for the “ridge”-like correlations, it is important to be able to calculate the two-particle correlation in the CGC framework beyond the lowest order. While some works do consider the role of small- x evolution and multiple rescatterings in the correlation function [11, 13, 38–40], most of the phenomenological approaches [11, 12, 41–43] simply include the saturation effects into the lowest-order calculation by evolving the unintegrated gluon distributions with the running-coupling BK (rcBK) nonlinear evolution [44–46].

The aim of this paper is to begin to analytically include saturation effects into the two-gluon correlation function in nucleus–nucleus collisions. Indeed full inclusion analytic of saturation effects originating in both nuclei would be a very hard problem: even the single gluon production in the quasi-classical MV limit of AA collisions can be dealt with only numerically at present [26, 27, 47, 48]. To make the problem more tractable we assume that one of the colliding nuclei is much larger than the other one, such that saturation effects are important only in interactions with the larger nucleus. In a more formal language [49, 50] for the quasi-classical MV model, we assume that $1 \ll A_1 \ll A_2$, where A_1 and A_2 are the atomic numbers of the smaller and larger nuclei, while $\alpha_s^2 A_2^{1/3} \sim 1$ and $\alpha_s^2 A_1^{1/3} \ll 1$. Equivalently one can say that we are interested in production of gluons with transverse momentum $k_T \gtrsim Q_{s1}$, where Q_{s1} is the saturation scale of the smaller nucleus. We do not impose any constraints on k_T compared to the saturation scale Q_{s2} of the larger nucleus ($Q_{s2} \gg Q_{s1} \gg \Lambda_{QCD}$). We stress here that this setup is not what is usually referred to as the pA collision in the saturation/CGC terminology: since $A_1 \gg 1$, the two gluon production cross section is dominated by the gluons produced in interactions of *different* nucleons in the smaller nucleus, which may also be viewed as a lowest-order saturation correction.

Below we calculate the two-gluon production cross section and the corresponding correlation function including the all-order saturation effects in the larger nucleus, while keeping them to the lowest non-trivial order in the smaller nucleus. The paper is structured as follows. In Sec. II we set up the problem. In the process of properly defining the correlation function we unexpectedly find a correlation originating in a simple fact that the nucleons in both nuclei are confined to within the nuclear radii. The effect is quite generic, and is not specific to the saturation/CGC approach used in the calculations in much of this paper: this correlation should be present in any model of AA collisions which properly takes into account the geometry of the collision. We refer to these correlations as the “geometric correlations”. We argue that this effect gives a non-trivial contribution to the correlator even if the two-gluon production cross section is given by disconnected Feynman diagrams, i.e., the correlation is not generated dynamically in the interactions. This correlation may be long-range in rapidity, though it does not have any non-trivial azimuthal structure.

The two-gluon production cross section in a heavy-light ion collision is calculated in Sec. III in terms of the Wilson line correlators. We show that the two-gluon production cross section is related to various correlators of four adjoint Wilson lines: the adjoint dipole, quadrupole, and a double-trace operator. These correlators contain both the multiple rescatterings of the quasi-classical MV approximation, along with the small- x BK/JIMWLK evolution.

We study the long-range rapidity correlations in Sec. IV. We evaluate the Wilson-line correlators describing the interaction with the target nucleus using the quasi-classical MV approximation and the large- N_c limit. By analyzing the two-gluon correlation function at the lowest non-trivial order, and in agreement with the earlier calculations in the literature [11, 13, 38, 40], we find both the near-side ($\Delta\phi = 0$) and away-side ($\Delta\phi = \pi$) long-range rapidity correlations. (Here $\Delta\phi$ is the azimuthal angle between the momenta of the produced gluons.) The two correlations are identical in their azimuthal shapes (as functions of $\Delta\phi$), such that the correlator can be expanded into a Fourier series in terms of only the even harmonics $\cos 2n \Delta\phi$. We discuss the possibility that such non-flow correlation may complicate experimental extraction of the contribution of the true QGP flow to the flow observables v_{2n} . In addition to the geometric and long-range rapidity correlations, the obtained two-gluon production cross section contains Hanbury-Brown–Twiss (HBT) correlations [51]. A somewhat peculiar feature of this HBT correlation is that it is accompanied by an identical back-to-back peak as well. We conclude in Sec. V by stressing the difference between near-side and away-side correlations calculated here and the mini-jet correlations: the near-side correlations in this work are long-range in rapidity, while the jet near-side correlations are local in rapidity.

II. CORRELATION FUNCTION AND “GEOMETRIC” CORRELATIONS

A. Definition of the correlator

Following a standard approach used in experimental analyses of particle correlations [5, 52] the correlation function can be defined as

$$C(\mathbf{k}_1, y_1, \mathbf{k}_2, y_2) = \mathcal{N} \frac{\frac{dN_{12}}{d^2k_1 dy_1 d^2k_2 dy_2}}{\frac{dN}{d^2k_1 dy_1} \frac{dN}{d^2k_2 dy_2}} - 1 \quad (1)$$

where

$$\frac{dN}{d^2k_1 dy_1} = \frac{1}{\sigma_{inel}} \frac{d\sigma}{d^2k_1 dy_1} \quad (2)$$

and

$$\frac{dN_{12}}{d^2k_1 dy_1 d^2k_2 dy_2} = \frac{1}{\sigma_{inel}} \frac{d\sigma}{d^2k_1 dy_1 d^2k_2 dy_2} \quad (3)$$

are the single- and double-particle multiplicity distributions with σ_{inel} the net inelastic nucleus–nucleus scattering cross section. Two-dimensional transverse vectors are denoted by $\mathbf{v} = (v^x, v^y)$ with their length $v_T \equiv |\mathbf{v}|$. The normalization factor \mathcal{N} in Eq. (1) is fixed by requiring that the number of particle pairs measured in the same (“real”) event N_{12} is equal to the number of (“mixed”) pairs with particles coming from different events $(N)^2$. Here we are interested in $\Delta\eta$ - $\Delta\phi$ correlations with $\Delta\phi = \phi_1 - \phi_2$ the difference between the azimuthal angles ϕ_1, ϕ_2 of the two momenta of the produced particles, and $\delta\eta = \eta_1 - \eta_2 \approx y_1 - y_2$ the difference between the pseudo-rapidities η_1, η_2 of the two particles. For such a correlation, with the magnitudes of the transverse momenta k_{1T} and k_{2T} constrained to some chosen data bins, the normalization factor is fixed by

$$\mathcal{N} \int d\phi_1 dy_1 d\phi_2 dy_2 \frac{dN_{12}}{d^2k_1 dy_1 d^2k_2 dy_2} = \int d\phi_1 dy_1 \frac{dN}{d^2k_1 dy_1} \int d\phi_2 dy_2 \frac{dN}{d^2k_2 dy_2}. \quad (4)$$

(We assume for simplicity that the number of produced particles is very large, $N \gg 1$, such that $N - 1 \approx N$ and σ_{inel} is the same in both Eqs. (2) and (3) since the production cross section of producing exactly one particle is negligible.)

Combining Eqs. (1), (2), (3), and (4) we rewrite the correlation function in terms of cross sections as

$$C(\mathbf{k}_1, y_1, \mathbf{k}_2, y_2) = \frac{\left[\int d\phi_1 dy_1 \frac{d\sigma}{d^2k_1 dy_1} \int d\phi_2 dy_2 \frac{d\sigma}{d^2k_2 dy_2} \right]}{\left[\int d\phi_1 dy_1 d\phi_2 dy_2 \frac{d\sigma}{d^2k_1 dy_1 d^2k_2 dy_2} \right]} \frac{\frac{d\sigma}{d^2k_1 dy_1 d^2k_2 dy_2}}{\frac{d\sigma}{d^2k_1 dy_1} \frac{d\sigma}{d^2k_2 dy_2}} - 1. \quad (5)$$

As outlined in the Introduction, we take one of the nuclei (the projectile) to be much smaller than the other, $A_1 \ll A_2$, such that saturation effects in it are minimal and nucleons in this (“first”) nucleus interact with the other (“second”) nucleus independent of each other. At the same time, the projectile nucleus is still large enough, $A_1 \gg 1$, such that the two-gluon production is dominated by the gluons generated by the interactions of two different nucleons from the first (projectile) nucleus with the second nucleus. (This interaction with the two nucleons in the first nucleus can be considered a lowest-order saturation effect.) Denote the 1- and 2-nucleon wave functions of the projectile nucleus A_1 by $\Psi_I(\mathbf{b})$ and $\Psi_{II}(\mathbf{b}_1, \mathbf{b}_2)$: they are normalized such that

$$\int d^2b |\Psi_I(\mathbf{b})|^2 = A_1, \quad \int d^2b_1 d^2b_2 |\Psi_{II}(\mathbf{b}_1, \mathbf{b}_2)|^2 = A_1 (A_1 - 1) \approx A_1^2. \quad (6)$$

With the help of these wave functions the single- and double-gluon production cross sections can be written as

$$\frac{d\sigma}{d^2k dy} = \int d^2B d^2b |\Psi_I(\mathbf{B} - \mathbf{b})|^2 \left\langle \frac{d\sigma^{pA_2}}{d^2k dy d^2b} \right\rangle \quad (7a)$$

$$\frac{d\sigma}{d^2k_1 dy_1 d^2k_2 dy_2} = \int d^2B d^2b_1 d^2b_2 |\Psi_{II}(\mathbf{B} - \mathbf{b}_1, \mathbf{B} - \mathbf{b}_2)|^2 \left\langle \frac{d\sigma^{pA_2}}{d^2k_1 dy_1 d^2b_1} \frac{d\sigma^{pA_2}}{d^2k_2 dy_2 d^2b_2} \right\rangle \quad (7b)$$

where \mathbf{B} is the impact parameter between the two nuclei and $\mathbf{b}, \mathbf{b}_1, \mathbf{b}_2$ the transverse positions of the nucleons in the projectile nucleus, all measured with respect to the center of the second (target) nucleus, as shown in Fig. 1 for the

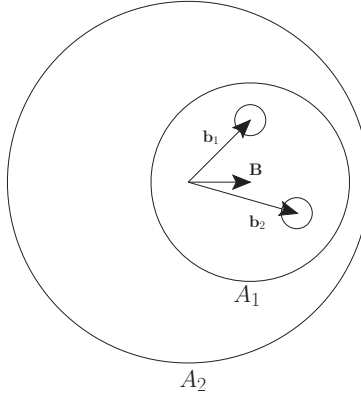


FIG. 1. Transverse plane geometry of the two-particle production in the collision of a smaller projectile nucleus (A_1) with a larger target nucleus (A_2). The two smaller circles represent two nucleons in the nucleus A_1 (see text for details).

two-gluon production process. (Transverse vector \mathbf{b} labels the position of the incoming nucleon in the single gluon production case, while \mathbf{b}_1 and \mathbf{b}_2 label positions of projectile nucleons for two-gluon production.) Here

$$\frac{d\sigma^{pA_2}}{d^2k dy d^2b}$$

is the cross section for the gluon production (with fixed transverse momentum \mathbf{k} , rapidity y , and transverse position \mathbf{b}) in the collision of a nucleon (p) with the target nucleus. The angle brackets $\langle \dots \rangle$ in (7) denote averaging in the target nucleus wave function along with summation over all the nucleons in the target nucleus [21–23, 33–36, 49]. Eqs. (7) can be used in Eq. (5) to give us the two-gluon correlation function in the heavy-light ion collision

$$C(\mathbf{k}_1, y_1, \mathbf{k}_2, y_2) = \frac{\left[\int d^2B d^2b_1 d\phi_1 dy_1 |\Psi_I(\mathbf{B} - \mathbf{b}_1)|^2 \left\langle \frac{d\sigma^{pA_2}}{d^2k_1 dy_1 d^2b_1} \right\rangle \right] \left[\int d^2B d^2b_2 d\phi_2 dy_2 |\Psi_I(\mathbf{B} - \mathbf{b}_2)|^2 \left\langle \frac{d\sigma^{pA_2}}{d^2k_2 dy_2 d^2b_2} \right\rangle \right]}{\left[\int d^2B d^2b_1 d^2b_2 d\phi_1 dy_1 d\phi_2 dy_2 |\Psi_{II}(\mathbf{B} - \mathbf{b}_1, \mathbf{B} - \mathbf{b}_2)|^2 \left\langle \frac{d\sigma^{pA_2}}{d^2k_1 dy_1 d^2b_1} \frac{d\sigma^{pA_2}}{d^2k_2 dy_2 d^2b_2} \right\rangle \right]} \\ \times \frac{\int d^2B d^2b_1 d^2b_2 |\Psi_{II}(\mathbf{B} - \mathbf{b}_1, \mathbf{B} - \mathbf{b}_2)|^2 \left\langle \frac{d\sigma^{pA_2}}{d^2k_1 dy_1 d^2b_1} \frac{d\sigma^{pA_2}}{d^2k_2 dy_2 d^2b_2} \right\rangle}{\left[\int d^2B d^2b_1 |\Psi_I(\mathbf{B} - \mathbf{b}_1)|^2 \left\langle \frac{d\sigma^{pA_2}}{d^2k_1 dy_1 d^2b_1} \right\rangle \right] \left[\int d^2B d^2b_2 |\Psi_I(\mathbf{B} - \mathbf{b}_2)|^2 \left\langle \frac{d\sigma^{pA_2}}{d^2k_2 dy_2 d^2b_2} \right\rangle \right]} - 1. \quad (8)$$

Here we model the nucleus as a bag of independent nucleons, which is a correct description at the leading order in the atomic number A [21–23, 49, 50, 53]. In such case the single-nucleon light-cone wave function squared is simply equal to the nuclear profile function in the projectile nucleus,¹

$$|\Psi_I(\mathbf{b})|^2 = T_1(\mathbf{b}). \quad (9)$$

(The nuclear profile function for a nucleus with density $\rho(\mathbf{b}, z)$ is defined by the integral over the longitudinal coordinate z ,

$$T(\mathbf{b}) = \int_{-\infty}^{\infty} dz \rho(\mathbf{b}, z), \quad (10)$$

such that for a spherical nucleus of radius R and constant density ρ it is $T(\mathbf{b}) = 2\rho\sqrt{R^2 - b^2}$.)

Without any loss of generality we can perform the integral over \mathbf{B} in Eq. (7a) obtaining

$$\frac{d\sigma}{d^2k dy} = A_1 \int d^2b \left\langle \frac{d\sigma^{pA_2}}{d^2k dy d^2b} \right\rangle. \quad (11)$$

¹ We do not show the spin and isospin indices explicitly in the wave functions: in our notation the wave function squared is implicitly averaged over all nucleon polarizations, since both colliding nuclei are unpolarized.

For a sufficiently large projectile nucleus, $A_1 \gg 1$, one can assume that the two-nucleon wave function can be factorized,

$$\Psi_{II}(\mathbf{b}_1, \mathbf{b}_2) = \Psi_I(\mathbf{b}_1) \Psi_I(\mathbf{b}_2), \quad (12)$$

such that, with the help of Eq. (9) we can write

$$|\Psi_{II}(\mathbf{b}_1, \mathbf{b}_2)|^2 = T_1(\mathbf{b}_1) T_1(\mathbf{b}_2). \quad (13)$$

Using this in Eq. (7b) we get

$$\frac{d\sigma}{d^2k_1 dy_1 d^2k_2 dy_2} = \int d^2B d^2b_1 d^2b_2 T_1(\mathbf{B} - \mathbf{b}_1) T_1(\mathbf{B} - \mathbf{b}_2) \left\langle \frac{d\sigma^{pA_2}}{d^2k_1 dy_1 d^2b_1} \frac{d\sigma^{pA_2}}{d^2k_2 dy_2 d^2b_2} \right\rangle \quad (14)$$

Substituting Eqs. (11) and (14) into Eq. (8) yields

$$C(\mathbf{k}_1, y_1, \mathbf{k}_2, y_2) = \frac{\left[\int d^2b_1 d\phi_1 dy_1 \left\langle \frac{d\sigma^{pA_2}}{d^2k_1 dy_1 d^2b_1} \right\rangle \right] \left[\int d^2b_2 d\phi_2 dy_2 \left\langle \frac{d\sigma^{pA_2}}{d^2k_2 dy_2 d^2b_2} \right\rangle \right]}{\left[\int d^2B d^2b_1 d^2b_2 d\phi_1 dy_1 d\phi_2 dy_2 T_1(\mathbf{B} - \mathbf{b}_1) T_1(\mathbf{B} - \mathbf{b}_2) \left\langle \frac{d\sigma^{pA_2}}{d^2k_1 dy_1 d^2b_1} \frac{d\sigma^{pA_2}}{d^2k_2 dy_2 d^2b_2} \right\rangle \right]} \\ \times \frac{\int d^2B d^2b_1 d^2b_2 T_1(\mathbf{B} - \mathbf{b}_1) T_1(\mathbf{B} - \mathbf{b}_2) \left\langle \frac{d\sigma^{pA_2}}{d^2k_1 dy_1 d^2b_1} \frac{d\sigma^{pA_2}}{d^2k_2 dy_2 d^2b_2} \right\rangle}{\int d^2b_1 \left\langle \frac{d\sigma^{pA_2}}{d^2k_1 dy_1 d^2b_1} \right\rangle \int d^2b_2 \left\langle \frac{d\sigma^{pA_2}}{d^2k_2 dy_2 d^2b_2} \right\rangle} - 1. \quad (15)$$

To complete the calculation one needs the single- and double-gluon production cross sections which, when used in Eq. (15), would give us the correlation function. Before we proceed to construct them, let us study a simple example elucidating the nature of one of the correlation types contained in correlator (15).

B. Geometric correlations

Let us consider the simplest possible example of particle (gluon) production mechanism where the interaction of the two nucleons in the first nucleus with the second nucleus in Eq. (14) factorizes,

$$\left\langle \frac{d\sigma^{pA_2}}{d^2k_1 dy_1 d^2b_1} \frac{d\sigma^{pA_2}}{d^2k_2 dy_2 d^2b_2} \right\rangle \approx \left\langle \frac{d\sigma^{pA_2}}{d^2k_1 dy_1 d^2b_1} \right\rangle \left\langle \frac{d\sigma^{pA_2}}{d^2k_2 dy_2 d^2b_2} \right\rangle. \quad (16)$$

This contribution comes from the disconnected Feynman diagrams and is usually identified as the uncorrelated part of the two-gluon production cross section. However, it is clear that substituting Eq. (16) into Eq. (15) does not reduce the correlation function to zero: instead one gets

$$C(\mathbf{k}_1, y_1, \mathbf{k}_2, y_2) = \frac{\left[\int d^2b_1 d\phi_1 dy_1 \left\langle \frac{d\sigma^{pA_2}}{d^2k_1 dy_1 d^2b_1} \right\rangle \right] \left[\int d^2b_2 d\phi_2 dy_2 \left\langle \frac{d\sigma^{pA_2}}{d^2k_2 dy_2 d^2b_2} \right\rangle \right]}{\left[\int d^2B d^2b_1 d^2b_2 d\phi_1 dy_1 d\phi_2 dy_2 T_1(\mathbf{B} - \mathbf{b}_1) T_1(\mathbf{B} - \mathbf{b}_2) \left\langle \frac{d\sigma^{pA_2}}{d^2k_1 dy_1 d^2b_1} \right\rangle \left\langle \frac{d\sigma^{pA_2}}{d^2k_2 dy_2 d^2b_2} \right\rangle \right]} \\ \times \frac{\int d^2B d^2b_1 d^2b_2 T_1(\mathbf{B} - \mathbf{b}_1) T_1(\mathbf{B} - \mathbf{b}_2) \left\langle \frac{d\sigma^{pA_2}}{d^2k_1 dy_1 d^2b_1} \right\rangle \left\langle \frac{d\sigma^{pA_2}}{d^2k_2 dy_2 d^2b_2} \right\rangle}{\int d^2b_1 \left\langle \frac{d\sigma^{pA_2}}{d^2k_1 dy_1 d^2b_1} \right\rangle \int d^2b_2 \left\langle \frac{d\sigma^{pA_2}}{d^2k_2 dy_2 d^2b_2} \right\rangle} - 1, \quad (17)$$

which, in general, could be non-zero.

Certainly if the \mathbf{b} -dependence factorizes from the rapidity and azimuthal dependence in the cross section

$$\left\langle \frac{d\sigma^{pA_2}}{d^2k dy d^2b} \right\rangle \quad (18)$$

then the correlation function (17) is zero: however, such factorization is not always the case. For gluon production in the saturation framework, the cross section is a complicated function of $k_T/Q_s(\mathbf{b}, y)$, which means it is not in a factorized form and thus the correlator (17) is not zero. Note that in the MV model (which does not contain the small- x evolution), gluon production is rapidity-independent, and, if one neglects the dependence of the gluon production cross section on the angle between \mathbf{k} and \mathbf{b} , the correlator (17) becomes zero. (Dependence of gluon production cross

section on the collision geometry in the MV approximation is not very strong, peaking at non-perturbatively low momenta [54].)

For the general case in Eq. (17) we observe a possible non-trivial correlation in the two-gluon production described by *disconnected* Feynman diagrams. If the gluon production cross section (18) is a slowly varying (but not constant) function of rapidity, as is the case in the saturation/CGC framework near mid-rapidity, this correlation would be long-range in rapidity. The origin of this correlation is somewhat peculiar: even though the two-nucleon wave function in Eq. (13) is factorized and, hence, represents uncorrelated nucleons, these two nucleons are correlated by the simple fact of being parts of the same bound state, the projectile nucleus. In other words, the probability of finding two nucleons at the impact parameters \mathbf{b}_1 and \mathbf{b}_2 is proportional to

$$\sim \int d^2B T_1(\mathbf{B} - \mathbf{b}_1) T_1(\mathbf{B} - \mathbf{b}_2) \quad (19)$$

and is not a product of two independent probabilities after all impact parameters \mathbf{B} of the incoming nucleus are integrated over: this is a correlation. Note also that the presence of real wave-function correlations, that is, non-factorizable corrections to the right-hand-side of Eq. (13), would also lead to some nontrivial two-particle correlations in Eq. (17).

If we define the correlation function at the fixed nuclear impact parameter \mathbf{B} by not integrating over \mathbf{B} in Eqs. (7) and using the result in Eq. (5), we get

$$C(\mathbf{k}_1, y_1, \mathbf{k}_2, y_2; \mathbf{B}) = \frac{\left[\int d^2b_1 d\phi_1 dy_1 |\Psi_I(\mathbf{B} - \mathbf{b}_1)|^2 \left\langle \frac{d\sigma^{pA_2}}{d^2k_1 dy_1 d^2b_1} \right\rangle \right] \left[\int d^2b_2 d\phi_2 dy_2 |\Psi_I(\mathbf{B} - \mathbf{b}_2)|^2 \left\langle \frac{d\sigma^{pA_2}}{d^2k_2 dy_2 d^2b_2} \right\rangle \right]}{\left[\int d^2b_1 d^2b_2 d\phi_1 dy_1 d\phi_2 dy_2 |\Psi_{II}(\mathbf{B} - \mathbf{b}_1, \mathbf{B} - \mathbf{b}_2)|^2 \left\langle \frac{d\sigma^{pA_2}}{d^2k_1 dy_1 d^2b_1} \frac{d\sigma^{pA_2}}{d^2k_2 dy_2 d^2b_2} \right\rangle \right]} \\ \times \frac{\int d^2b_1 d^2b_2 |\Psi_{II}(\mathbf{B} - \mathbf{b}_1, \mathbf{B} - \mathbf{b}_2)|^2 \left\langle \frac{d\sigma^{pA_2}}{d^2k_1 dy_1 d^2b_1} \frac{d\sigma^{pA_2}}{d^2k_2 dy_2 d^2b_2} \right\rangle}{\int d^2b_1 |\Psi_I(\mathbf{B} - \mathbf{b}_1)|^2 \left\langle \frac{d\sigma^{pA_2}}{d^2k_1 dy_1 d^2b_1} \right\rangle \int d^2b_2 |\Psi_I(\mathbf{B} - \mathbf{b}_2)|^2 \left\langle \frac{d\sigma^{pA_2}}{d^2k_2 dy_2 d^2b_2} \right\rangle} - 1, \quad (20)$$

One can see that this fixed-impact parameter correlation function in Eq. (20) is zero, $C(\mathbf{B}) = 0$, for the factorized wave function from Eq. (13) and for disconnected-diagram interactions from Eq. (16). Thus di-gluon correlations due to our “geometric” correlation mechanism seem to also disappear when the impact parameter is fixed exactly. However, such precise determination of the impact parameter is impossible in an experimental analysis, where one is able to fix the collision centrality $|\mathbf{B}|$ in a certain interval, but one can not fix the direction of \mathbf{B} . The integration over any range of the impact parameter $|\mathbf{B}|$ (or the integration over the angles of \mathbf{B} keeping $|\mathbf{B}|$ constant) is likely to introduce these geometric correlations, as follows from Eq. (15). Note that the presence of non-trivial wave function correlations, i.e., correlations beyond the factorization approximation in Eq. (13), may also lead to correlations which may survive in Eq. (20) even for a fixed impact parameter \mathbf{B} and uncorrelated interactions (16).

Despite its simplicity, the non-vanishing correlation in Eq. (17) is one of the main results of this work. In the saturation/CGC framework it may lead to long-range rapidity correlations similar to the observed “ridge” correlation. Indeed azimuthal correlations are missing in Eq. (17): such correlations may be formed in heavy ion collisions due to radial flow, as was argued in [8]. Indeed a lot more work is needed to compare this result with experiment.

III. TWO-GLUON PRODUCTION AND CORRELATIONS

In this Section we are going to calculate the two-gluon production cross section for the heavy-light ion collisions working in the saturation/CGC framework. As described above we assume that $A_2 \gg A_1 \gg 1$, such that the saturation effects are resummed to all orders only in the target nucleus with atomic number A_2 . While the saturation effects are not very important in the projectile nucleus with the atomic number A_1 , the fact that $A_1 \gg 1$ implies that the two gluons are predominantly produced in collisions of different nucleons in the projectile nucleus with the target nucleus.

According to the standard technique [16, 20], the calculation will proceed using the light-cone perturbation theory (LCPT) [55, 56] to construct the gluon wave functions in the incoming projectile nucleus. The production cross section will be obtained by convoluting the square of this light-cone wave function with the interaction with the target nucleus, which will be described by Wilson lines along the light cone [17, 29], which include the saturation effects in the form of both the Glauber–Mueller multiple rescatterings [53] and the BK/JIMWLK evolution equations.

The diagrams contributing to the scattering amplitude of the two-gluon production in the collision of two nucleons from the projectile nucleus with the target nucleus are shown in Fig. 2. There the two nucleons in the incoming nucleus

are denoted by horizontal solid lines representing two quarks in the wave functions of those nucleons: throughout this work we will model the nucleons by a single valence quark each. (Generalization of our results to a more realistic nucleon wave function is straightforward.) Interaction with the target, which happens over a time-scale much shorter than the time scale of preparing gluons in the wave functions, is denoted by a vertical dashed line.

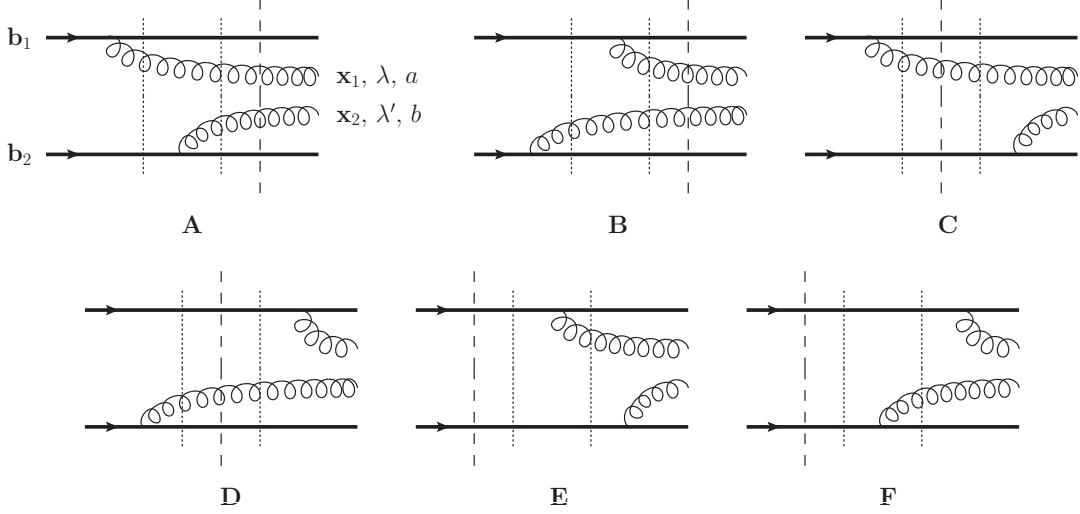


FIG. 2. Diagrams describing the two-gluon production in the heavy-light ion collision. Two horizontal solid lines denote valence quarks inside the two nucleons in the projectile nucleus. Vertical dashed line denotes the interaction with the target nucleus, while the vertical dotted lines denote intermediate states.

A. Light cone wave functions of the gluons

An essential part of the calculation is finding the light cone wave functions of the two interacting nucleons generating gluons in the incoming nucleus. The diagrams in Fig. 2 include vertical dotted lines denoting the intermediate states contributing light-cone energy denominators to the wave functions. The energy denominators, and hence the wave functions of the two nucleons, factorize. While this is obvious in diagrams C and D in Fig. 2, we will explain this factorization for other diagrams in a little more detail below.

We assume that the projectile nucleus is moving along the light cone “+” direction and the nucleons carry very large $p^+ = (p^0 + p^3)/\sqrt{2}$ momenta. At the same time, the gluons carry light cone momenta k_1^+ and k_2^+ such that $p^+ \gg k_1^+, k_2^+$. The gluons will be produced with rapidities far away from the fragmentation regions of the colliding nuclei. The small light cone momenta of the gluons make them dominate the energy denominators, generating a much larger contribution than that of the (valence) quarks [57].

The only difference between the diagrams A and B in Fig. 2 is the ordering of the emitted gluons. This will only affect the energy denominators that result from the light-cone perturbation theory rules [55, 56]. When these two diagrams are added together these energy denominators factorize. Denoting the light cone energies of the two gluons in diagrams A and B by E_1 and E_2 such that $E_1 = k_{1T}^2/(2k_1^+)$ and $E_2 = k_{2T}^2/(2k_2^+)$ we see that adding the contributions of the energy denominators in those graphs gives

$$\frac{1}{E_1} \frac{1}{E_1 + E_2} + \frac{1}{E_2} \frac{1}{E_1 + E_2} = \frac{1}{E_1} \frac{1}{E_2}. \quad (21)$$

The result factorizes into the terms describing one or another gluon. Analysis of the diagrams E and F leads to the same factorization of energy denominators [58].

The two-gluon light cone wave function for diagrams A+B and E+F is

$$\psi^{ab}(\mathbf{x}_1, \mathbf{b}_1, \lambda; \mathbf{x}_2, \mathbf{b}_2, \lambda') = \psi^a(\mathbf{x}_1, \mathbf{b}_1, \lambda) \psi^b(\mathbf{x}_2, \mathbf{b}_2, \lambda') = -\frac{g^2}{\pi^2} (t^a)_1 (t^b)_2 \frac{(\mathbf{x}_1 - \mathbf{b}_1) \cdot \boldsymbol{\epsilon}_\lambda^*}{|\mathbf{x}_1 - \mathbf{b}_1|^2} \frac{(\mathbf{x}_2 - \mathbf{b}_2) \cdot \boldsymbol{\epsilon}_{\lambda'}^*}{|\mathbf{x}_2 - \mathbf{b}_2|^2} \quad (22)$$

where g is the QCD coupling constant and the polarization vector is $\boldsymbol{\epsilon}_\lambda = -(1/\sqrt{2})(\lambda, i)$ [55, 56]. The factors of $(t^a)_i$ are the $SU(N_c)$ generators in the fundamental representation with N_c the number of quark colors, while the subscript

$i = 1, 2$ denotes the associated nucleons. The single nucleon's soft gluon wave function is [57]

$$\psi^a(\mathbf{x}, \mathbf{b}, \lambda) = \frac{ig}{\pi} t^a \frac{(\mathbf{x} - \mathbf{b}) \cdot \boldsymbol{\epsilon}_\lambda^*}{|\mathbf{x} - \mathbf{b}|^2}. \quad (23)$$

The diagrams C+D have a wave function different from Eq. (22) by a minus sign. The minus sign difference will be absorbed in the interaction term.

B. Single gluon production

Our calculation for the two-gluon production cross section will be closely following that for the single gluon production in a collision of a single nucleon with a nucleus (a pA collision). For this reason, and also because we need the single inclusive gluon production cross section to construct the correlator (15), let us briefly review the results.

The single-gluon inclusive production cross section in pA collisions is illustrated in Fig. 3, which shows the square of the scattering amplitude. The cross denotes the measured gluon. The vertical solid straight line in Fig. 3 is the final-state cut, while the vertical dashed lines denote interactions with the target just like in Fig. 2.

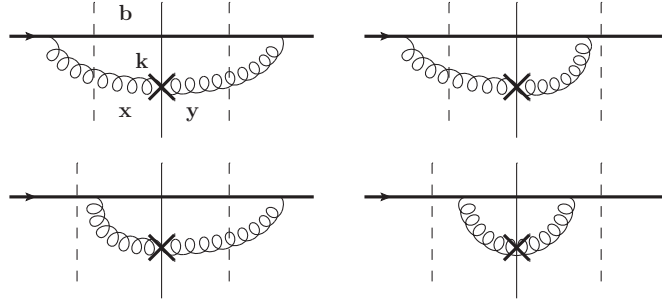


FIG. 3. Diagrams contributing to the square of the scattering amplitude for the single gluon production in pA collisions. The cross denotes the measured produced gluon.

The gluon production cross section can be written as [59–62] (with the projectile proton represented by a single valence quark)

$$\left\langle \frac{d\sigma^{pA_2}}{d^2k dy d^2b} \right\rangle = \frac{1}{2(2\pi)^3} \int d^2x d^2y e^{-i\mathbf{k} \cdot (\mathbf{x} - \mathbf{y})} \sum_{\lambda, a} \psi^a(\mathbf{x}, \mathbf{b}, \lambda) \psi^{a*}(\mathbf{y}, \mathbf{b}, \lambda) \text{Int}_1(\mathbf{x}, \mathbf{y}, \mathbf{b}) \quad (24)$$

with the coordinate notation defined in Fig. 3. The wave function squared summed over polarizations and colors is

$$\sum_{\lambda, a} \psi^a(\mathbf{x}, \mathbf{b}, \lambda) \psi^{a*}(\mathbf{y}, \mathbf{b}, \lambda) = \frac{4\alpha_s C_F}{\pi} \frac{\mathbf{x} - \mathbf{b}}{|\mathbf{x} - \mathbf{b}|^2} \cdot \frac{\mathbf{y} - \mathbf{b}}{|\mathbf{y} - \mathbf{b}|^2} \quad (25)$$

with $C_F = (N_c^2 - 1)/(2N_c)$ the fundamental-representation Casimir operator, while the interaction with the target is

$$\text{Int}_1(\mathbf{x}, \mathbf{y}, \mathbf{b}) = \left\langle \frac{1}{N_c^2 - 1} \text{Tr}[U_{\mathbf{x}} U_{\mathbf{y}}^\dagger] - \frac{1}{N_c^2 - 1} \text{Tr}[U_{\mathbf{x}} U_{\mathbf{b}}^\dagger] - \frac{1}{N_c^2 - 1} \text{Tr}[U_{\mathbf{b}} U_{\mathbf{y}}^\dagger] + 1 \right\rangle. \quad (26)$$

The latter object is written in terms of expectation values (in the target nucleus wave function) of the adjoint Wilson lines along the x^+ light cone:

$$U_{\mathbf{x}} = \text{P exp} \left\{ i g \int_{-\infty}^{\infty} dx^+ \mathcal{A}^-(x^+, x^- = 0, \mathbf{x}) \right\}, \quad (27)$$

where \mathcal{A}^μ is the gluon field of the target in the adjoint representation.

Defining the adjoint (gluon) dipole S -matrix by

$$S_G(\mathbf{x}_1, \mathbf{x}_2, y) \equiv \frac{1}{N_c^2 - 1} \langle \text{Tr}[U_{\mathbf{x}_1} U_{\mathbf{x}_2}^\dagger] \rangle \quad (28)$$

we rewrite Eq. (24) as

$$\left\langle \frac{d\sigma^{pA_2}}{d^2k dy d^2b} \right\rangle = \frac{\alpha_s C_F}{4\pi^4} \int d^2x d^2y e^{-i\mathbf{k}\cdot(\mathbf{x}-\mathbf{y})} \frac{\mathbf{x}-\mathbf{b}}{|\mathbf{x}-\mathbf{b}|^2} \cdot \frac{\mathbf{y}-\mathbf{b}}{|\mathbf{y}-\mathbf{b}|^2} [S_G(\mathbf{x}, \mathbf{y}, y) - S_G(\mathbf{x}, \mathbf{b}, y) - S_G(\mathbf{b}, \mathbf{y}, y) + 1]. \quad (29)$$

Using Eq. (29) in Eq. (11) we obtain the gluon production cross section in the heavy-light ion collision.

The dipole amplitude S_G in Eq. (29) contains the Glauber-Mueller multiple rescatterings [53] (recovered by putting $y = 0$ in the argument of S_G), along with the energy dependence included though the BK/JIMWLK evolution equations [58, 62]: the cross section formula remains the same in both cases. The former case would correspond to consistently treating the problem in the MV model [59–61]. The latter case would include small- x evolution corrections in the rapidity interval between the produced gluon and the target nucleus: one may worry that such inclusion would be asymmetric, since the evolution in the rapidity range between the projectile and the produced target is not included. A more symmetric treatment of the gluon production problem in pA collisions with evolution corrections included in all rapidity intervals is presented in [58] (see also [16, 20] for a more pedagogical presentation). Inclusion of evolution in the rapidity interval between the projectile and the produced gluon(s) is beyond the scope of the present work: it should be possible along the lines of [58] though.

C. Two-gluon production with long-range rapidity correlations: “square” of the single gluon production

The two-gluon production in heavy-light ion collisions is easily constructed by analogy to the single-gluon production calculation of Sec. III B. The diagrams contributing to the square of the scattering amplitude for the double gluon production in heavy-light ion collisions are shown in Fig. 4, written as a direct product of the gluon production processes in the interactions of each of the nucleons from the projectile nucleus with the target. Just as in Fig. 3 the vertical dashed lines in Fig. 4 represent interactions with the target, while the vertical solid line denotes the final state cut.

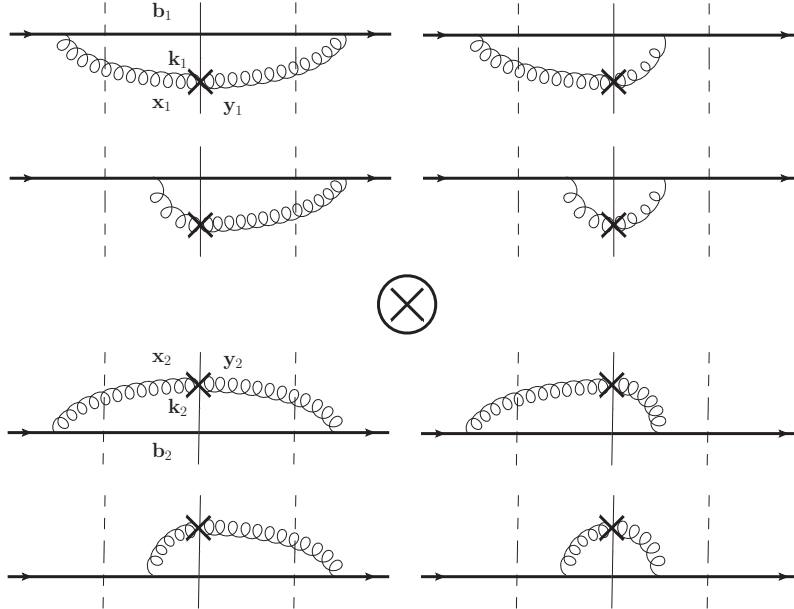


FIG. 4. Diagrams contributing to the two-gluon production cross section in the heavy-light ion collision. For clarity the diagrams are shown as a direct product of gluon production processes in collisions of the two interacting nucleons from the projectile nucleus with the target nucleus.

The evaluation of the diagrams in Fig. 4 is straightforward. The two-gluon wave function squared is obtained by using Eq. (25) twice, which yields

$$\begin{aligned} & \sum_{\lambda, \lambda', a, b} \psi^{ab}(x_1, b_1, \lambda; x_2, b_2, \lambda') \psi^{ab*}(y_1, b_1, \lambda; y_2, b_2, \lambda') \\ &= \frac{16 \alpha_s^2 C_F^2}{\pi^2} \frac{x_1 - b_1}{|x_1 - b_1|^2} \cdot \frac{y_1 - b_1}{|y_1 - b_1|^2} \frac{x_2 - b_2}{|x_2 - b_2|^2} \cdot \frac{y_2 - b_2}{|y_2 - b_2|^2} \end{aligned} \quad (30)$$

with all the coordinate labels explained in Fig. 4.

Interactions with the target are treated similarly. The traces of Wilson lines in the top and bottom parts of Fig. 4 are exactly the same as in Eq. (26) and appear to factorize, suggesting absence of dynamically generated correlations. This is not so. Note, that the averaging over the target is applied to both parts of Fig. 4 simultaneously: we thus get an averaged product of traces of Wilson lines,

$$Int_2(\mathbf{x}_1, \mathbf{y}_1, \mathbf{b}_1; \mathbf{x}_2, \mathbf{y}_2, \mathbf{b}_2) = \left\langle \left(\frac{1}{N_c^2 - 1} Tr[U_{\mathbf{x}_1} U_{\mathbf{y}_1}^\dagger] - \frac{1}{N_c^2 - 1} Tr[U_{\mathbf{x}_1} U_{\mathbf{b}_1}^\dagger] - \frac{1}{N_c^2 - 1} Tr[U_{\mathbf{b}_1} U_{\mathbf{y}_1}^\dagger] + 1 \right) \right. \\ \left. \times \left(\frac{1}{N_c^2 - 1} Tr[U_{\mathbf{x}_2} U_{\mathbf{y}_2}^\dagger] - \frac{1}{N_c^2 - 1} Tr[U_{\mathbf{x}_2} U_{\mathbf{b}_2}^\dagger] - \frac{1}{N_c^2 - 1} Tr[U_{\mathbf{b}_2} U_{\mathbf{y}_2}^\dagger] + 1 \right) \right\rangle, \quad (31)$$

which does not, in general, factorize into the product of two separately target-averaged interactions from Eq. (26).

Using Eq. (14) we write

$$\frac{d\sigma_{square}}{d^2 k_1 dy_1 d^2 k_2 dy_2} = \frac{1}{[2(2\pi)^3]^2} \int d^2 B d^2 b_1 d^2 b_2 T_1(\mathbf{B} - \mathbf{b}_1) T_1(\mathbf{B} - \mathbf{b}_2) d^2 x_1 d^2 y_1 d^2 x_2 d^2 y_2 e^{-i \mathbf{k}_1 \cdot (\mathbf{x}_1 - \mathbf{y}_1) - i \mathbf{k}_2 \cdot (\mathbf{x}_2 - \mathbf{y}_2)} \\ \times \sum_{\lambda, \lambda', a, b} \psi^{ab}(\mathbf{x}_1, \mathbf{b}_1, \lambda; \mathbf{x}_2, \mathbf{b}_2, \lambda') \psi^{ab*}(\mathbf{y}_1, \mathbf{b}_1, \lambda; \mathbf{y}_2, \mathbf{b}_2, \lambda') Int_2(\mathbf{x}_1, \mathbf{y}_1, \mathbf{b}_1; \mathbf{x}_2, \mathbf{y}_2, \mathbf{b}_2), \quad (32)$$

which, with the help of Eqs. (30) and (31) becomes (cf. [40])

$$\frac{d\sigma_{square}}{d^2 k_1 dy_1 d^2 k_2 dy_2} = \frac{\alpha_s^2 C_F^2}{16 \pi^8} \int d^2 B d^2 b_1 d^2 b_2 T_1(\mathbf{B} - \mathbf{b}_1) T_1(\mathbf{B} - \mathbf{b}_2) d^2 x_1 d^2 y_1 d^2 x_2 d^2 y_2 e^{-i \mathbf{k}_1 \cdot (\mathbf{x}_1 - \mathbf{y}_1) - i \mathbf{k}_2 \cdot (\mathbf{x}_2 - \mathbf{y}_2)} \\ \times \frac{\mathbf{x}_1 - \mathbf{b}_1}{|\mathbf{x}_1 - \mathbf{b}_1|^2} \cdot \frac{\mathbf{y}_1 - \mathbf{b}_1}{|\mathbf{y}_1 - \mathbf{b}_1|^2} \cdot \frac{\mathbf{x}_2 - \mathbf{b}_2}{|\mathbf{x}_2 - \mathbf{b}_2|^2} \cdot \frac{\mathbf{y}_2 - \mathbf{b}_2}{|\mathbf{y}_2 - \mathbf{b}_2|^2} \\ \times \left\langle \left(\frac{1}{N_c^2 - 1} Tr[U_{\mathbf{x}_1} U_{\mathbf{y}_1}^\dagger] - \frac{1}{N_c^2 - 1} Tr[U_{\mathbf{x}_1} U_{\mathbf{b}_1}^\dagger] - \frac{1}{N_c^2 - 1} Tr[U_{\mathbf{b}_1} U_{\mathbf{y}_1}^\dagger] + 1 \right) \right. \\ \left. \times \left(\frac{1}{N_c^2 - 1} Tr[U_{\mathbf{x}_2} U_{\mathbf{y}_2}^\dagger] - \frac{1}{N_c^2 - 1} Tr[U_{\mathbf{x}_2} U_{\mathbf{b}_2}^\dagger] - \frac{1}{N_c^2 - 1} Tr[U_{\mathbf{b}_2} U_{\mathbf{y}_2}^\dagger] + 1 \right) \right\rangle. \quad (33)$$

This is the expression for the two-gluon production cross section coming from the diagrams in Fig. 4. The interaction with the target can be evaluated in the quasi-classical multiple rescattering approximation, as we will show later. The rapidity evolution can be included using the JIMWLK equation. Note, however, that when the rapidity difference between the two gluons is sufficiently large, $|y_1 - y_2| \gtrsim 1/\alpha_s$, one has to include the evolution corrections in the rapidity interval between the produced gluons, such that the Wilson lines in the two parenthesis in Eq. (33) should be taken at different rapidities. A similar effect had to be included in the two-gluon production cross section in DIS in [63]. In such regime one would also need to include evolution corrections in the rapidity window between the projectile and (at least one of) the produced gluons. Inclusion of the evolution corrections in terms of the weight functional W of the JIMWLK evolution equation into the two-gluon production cross section in nucleus–nucleus collisions was done in [11]. In this work we will limit ourselves to the quasi-classical regime where no evolution corrections are required and the cross sections are rapidity-independent.

Note that for scattering on a large nuclear target, if one resums powers of $\alpha_s^2 A^{1/3}$, as is the case in the Glauber-Mueller (GM) rescatterings (and in the BK/JIMWLK evolution for which the GM rescatterings serve as the initial condition), and if one takes the large- N_c limit, the expectation values of the traces in Eq. (33) factorize, such that

$$\left\langle Tr[U_{\mathbf{x}_1} U_{\mathbf{y}_1}^\dagger] Tr[U_{\mathbf{x}_2} U_{\mathbf{y}_2}^\dagger] \right\rangle \Big|_{\text{large-}N_c, \text{large-}A_2} \approx \langle Tr[U_{\mathbf{x}_1} U_{\mathbf{y}_1}^\dagger] \rangle \langle Tr[U_{\mathbf{x}_2} U_{\mathbf{y}_2}^\dagger] \rangle. \quad (34)$$

This leads to factorization of Eq. (16) being valid in the large- N_c and large-target-nucleus limit. As shown above, even in this factorized regime one may obtain a non-trivial correlation function due to the geometric correlations.

D. Two-gluon production with long-range rapidity correlations: “crossed” diagrams

Before we proceed to evaluating the correlations contained in the cross section (33), let us point out another contribution to the two-gluon production cross section arising from squaring the sum of the diagrams in Fig. 2. When squaring the diagrams in Fig. 2 it is possible that the gluon emitted by one nucleon in the amplitude will be absorbed

by another nucleon in the complex conjugate amplitude. The corresponding contributions to the cross section are shown in Figs. 5 and 6, where crossing gluon lines do not form a vertex. We will refer to these diagrams as the “crossed” graphs. The diagrams obtained from those in Figs. 5 and 6 by a mirror reflection with respect to the cut correspond to the $\mathbf{b}_1 \leftrightarrow \mathbf{b}_2$ interchange, and will be automatically included in the cross section to be calculated below since it will contain integrals over all \mathbf{b}_1 and \mathbf{b}_2 . The sum over different orderings of gluon emissions in the (complex conjugate) amplitude of Fig. 6 is implied, but is not shown explicitly.

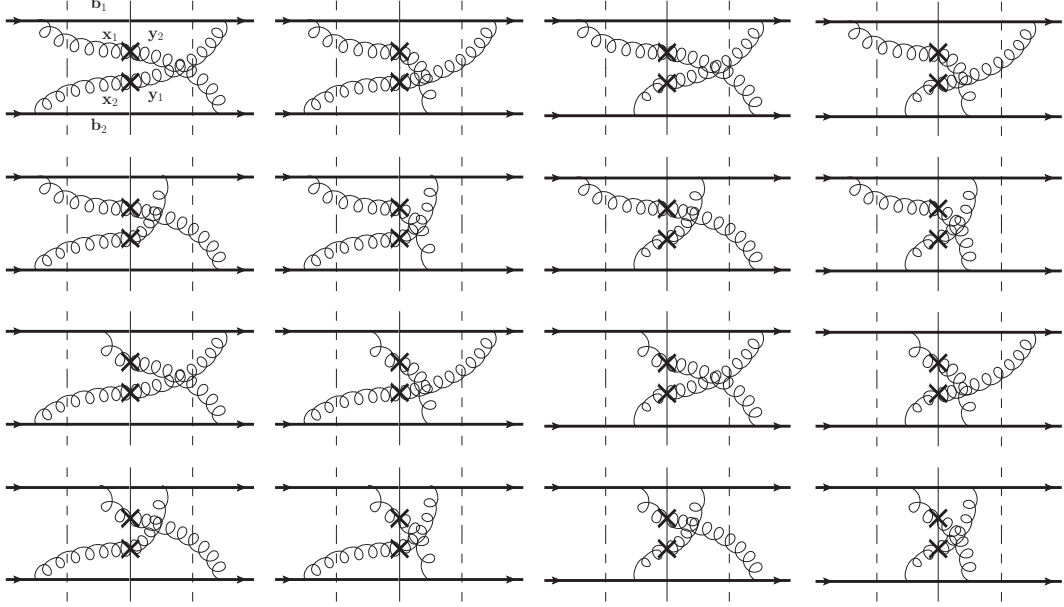


FIG. 5. Diagrams contributing to the two-gluon production cross section, with the gluon emitted by each nucleon in the amplitude absorbed by another nucleon in the complex conjugate amplitude. The top cross denotes the gluon with momentum \mathbf{k}_1 , while the bottom one denotes the gluon with momentum \mathbf{k}_2 .

In evaluating the graphs in Figs. 5 and 6 we note that there are non-trivial color factors due to the interaction terms, which we absorb into the wave function. The expression for the wave function squared is

$$\frac{16}{\pi^2} \frac{\alpha_s^2}{2N_c} \frac{C_F}{|\mathbf{x}_1 - \mathbf{b}_1|^2} \cdot \frac{\mathbf{y}_2 - \mathbf{b}_2}{|\mathbf{y}_2 - \mathbf{b}_2|^2} \frac{\mathbf{x}_2 - \mathbf{b}_2}{|\mathbf{x}_2 - \mathbf{b}_2|^2} \cdot \frac{\mathbf{y}_1 - \mathbf{b}_1}{|\mathbf{y}_1 - \mathbf{b}_1|^2}. \quad (35)$$

Defining the color-quadrupole operator [63–67]

$$Q(\mathbf{x}_1, \mathbf{x}_2, \mathbf{x}_3, \mathbf{x}_4) \equiv \frac{1}{N_c^2 - 1} \langle \text{Tr}[U_{\mathbf{x}_1} U_{\mathbf{x}_2}^\dagger U_{\mathbf{x}_3} U_{\mathbf{x}_4}^\dagger] \rangle \quad (36)$$

after some algebra the interactions with the target in both Fig. 5 and Fig. 6 can be shown to be equal to (with the terms ordered in the same way as the diagrams in Figs. 5 and 6 and the transverse coordinates defined in the upper left diagram of each of these two figures)

$$\begin{aligned} \text{Int}_{\text{crossed}}(\mathbf{x}_1, \mathbf{y}_1, \mathbf{b}_1, \mathbf{x}_2, \mathbf{y}_2, \mathbf{b}_2) = & Q(\mathbf{x}_1, \mathbf{y}_1, \mathbf{x}_2, \mathbf{y}_2) - Q(\mathbf{x}_1, \mathbf{y}_1, \mathbf{x}_2, \mathbf{b}_2) - Q(\mathbf{x}_1, \mathbf{y}_1, \mathbf{b}_2, \mathbf{y}_2) + S_G(\mathbf{x}_1, \mathbf{y}_1) \\ & - Q(\mathbf{x}_1, \mathbf{b}_1, \mathbf{x}_2, \mathbf{y}_2) + Q(\mathbf{x}_1, \mathbf{b}_1, \mathbf{x}_2, \mathbf{b}_2) + Q(\mathbf{x}_1, \mathbf{b}_1, \mathbf{b}_2, \mathbf{y}_2) - S_G(\mathbf{x}_1, \mathbf{b}_1) \\ & - Q(\mathbf{b}_1, \mathbf{y}_1, \mathbf{x}_2, \mathbf{y}_2) + Q(\mathbf{b}_1, \mathbf{y}_1, \mathbf{x}_2, \mathbf{b}_2) + Q(\mathbf{b}_1, \mathbf{y}_1, \mathbf{b}_2, \mathbf{y}_2) - S_G(\mathbf{b}_1, \mathbf{y}_1) \\ & + S_G(\mathbf{x}_2, \mathbf{y}_2) - S_G(\mathbf{x}_2, \mathbf{b}_2) - S_G(\mathbf{b}_2, \mathbf{y}_2) + 1. \end{aligned} \quad (37)$$

The only difference between the contributions of the diagrams in Figs. 5 and 6 is in the exponential factors for the Fourier transform into the transverse momentum space.

The longitudinal momentum flow patterns in Figs. 5 and 6 are different from that in Fig. 4. This is illustrated in Fig. 7, which shows the flow of the “plus” momentum component through the first diagram in Fig. 5. Note that the change in the “plus” momentum component is negligible in the eikonal interactions with the target considered here. Requiring that the incoming quark lines carry the same “plus” momentum both in the amplitude and in the complex

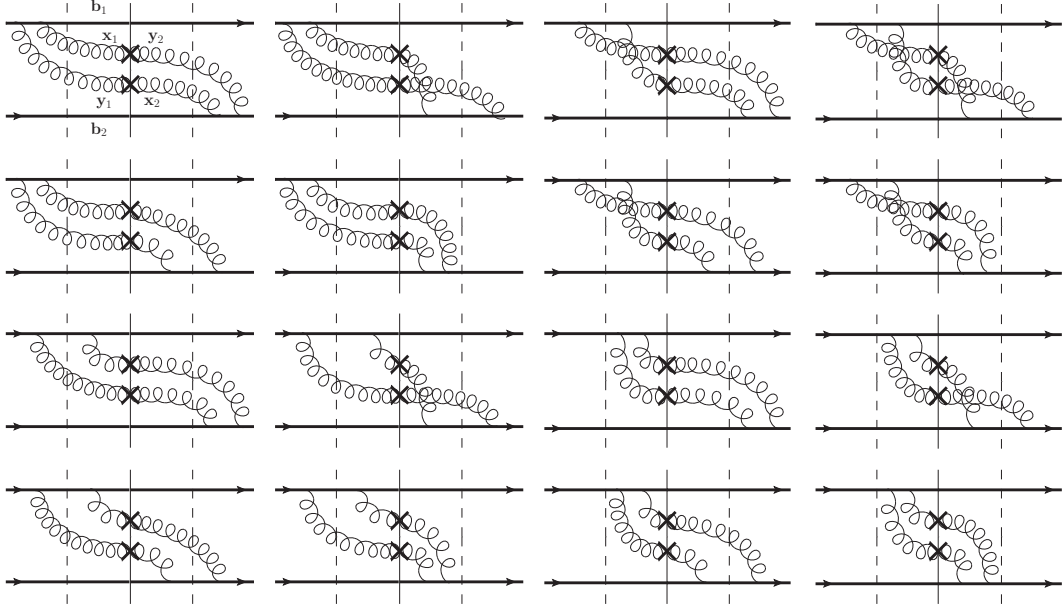


FIG. 6. Another set of diagrams contributing to the two-gluon production cross section, with the gluon emitted by each nucleon in the amplitude absorbed by another nucleon in the complex conjugate amplitude. Again the top cross denotes the gluon with momentum k_1 , while the bottom one denotes the gluon with momentum k_2 . Summation over the different orderings of gluon emissions (e.g. which gluon is emitted first or second) is implied but is not shown explicitly.

conjugate amplitude, one would obtain $k_1^+ = k_2^+$: however such requirement is not correct. The actual scattering happens between two nuclei, and it is the momenta of the whole incoming nuclei which have to be equal both in the amplitude and in the complex conjugate amplitude. Hence for $k_1^+ \neq k_2^+$ the diagrams like that in Fig. 7 would only correspond to different redistributions of the projectile nucleus momentum between the nucleons in it in the amplitude and in the complex conjugate amplitude without changing the same “plus” momentum of the whole nucleus on both sides of the cut. Hence the $k_1^+ = k_2^+$ condition is not necessary for the “crossed” diagrams.

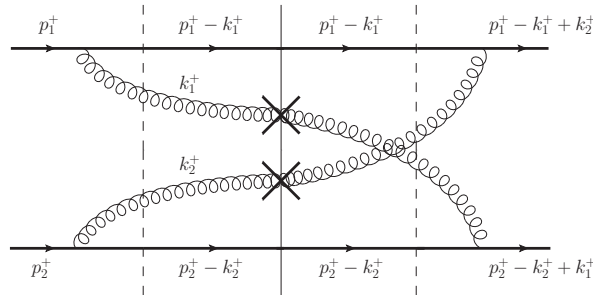


FIG. 7. The flow of the “plus” momentum component through the first diagram in Fig. 5.

Combining the factors in Eqs. (35) and (37), and inserting Fourier transform exponentials, we arrive at the expression

for the two-gluon production cross section contribution resulting from the “crossed” diagrams from Figs. 5 and 6

$$\begin{aligned}
\frac{d\sigma_{crossed}}{d^2k_1 dy_1 d^2k_2 dy_2} &= \frac{1}{[2(2\pi)^3]^2} \int d^2B d^2b_1 d^2b_2 T_1(\mathbf{B} - \mathbf{b}_1) T_1(\mathbf{B} - \mathbf{b}_2) d^2x_1 d^2y_1 d^2x_2 d^2y_2 \\
&\times \left[e^{-i\mathbf{k}_1 \cdot (\mathbf{x}_1 - \mathbf{y}_2) - i\mathbf{k}_2 \cdot (\mathbf{x}_2 - \mathbf{y}_1)} + e^{-i\mathbf{k}_1 \cdot (\mathbf{x}_1 - \mathbf{y}_2) + i\mathbf{k}_2 \cdot (\mathbf{x}_2 - \mathbf{y}_1)} \right] \frac{16\alpha_s^2}{\pi^2} \frac{C_F}{2N_c} \frac{\mathbf{x}_1 - \mathbf{b}_1}{|\mathbf{x}_1 - \mathbf{b}_1|^2} \cdot \frac{\mathbf{y}_2 - \mathbf{b}_2}{|\mathbf{y}_2 - \mathbf{b}_2|^2} \frac{\mathbf{x}_2 - \mathbf{b}_2}{|\mathbf{x}_2 - \mathbf{b}_2|^2} \cdot \frac{\mathbf{y}_1 - \mathbf{b}_1}{|\mathbf{y}_1 - \mathbf{b}_1|^2} \\
&\times \left[Q(\mathbf{x}_1, \mathbf{y}_1, \mathbf{x}_2, \mathbf{y}_2) - Q(\mathbf{x}_1, \mathbf{y}_1, \mathbf{x}_2, \mathbf{b}_2) - Q(\mathbf{x}_1, \mathbf{y}_1, \mathbf{b}_2, \mathbf{y}_2) + S_G(\mathbf{x}_1, \mathbf{y}_1) - Q(\mathbf{x}_1, \mathbf{b}_1, \mathbf{x}_2, \mathbf{y}_2) + Q(\mathbf{x}_1, \mathbf{b}_1, \mathbf{x}_2, \mathbf{b}_2) \right. \\
&+ Q(\mathbf{x}_1, \mathbf{b}_1, \mathbf{b}_2, \mathbf{y}_2) - S_G(\mathbf{x}_1, \mathbf{b}_1) - Q(\mathbf{b}_1, \mathbf{y}_1, \mathbf{x}_2, \mathbf{y}_2) + Q(\mathbf{b}_1, \mathbf{y}_1, \mathbf{x}_2, \mathbf{b}_2) + Q(\mathbf{b}_1, \mathbf{y}_1, \mathbf{b}_2, \mathbf{y}_2) - S_G(\mathbf{b}_1, \mathbf{y}_1) + S_G(\mathbf{x}_2, \mathbf{y}_2) \\
&\left. - S_G(\mathbf{x}_2, \mathbf{b}_2) - S_G(\mathbf{b}_2, \mathbf{y}_2) + 1 \right]. \tag{38}
\end{aligned}$$

Just like in Eq. (33), the dipole and quadrupole scattering amplitudes in Eq. (38) can be evaluated either in the MV model or by using BK and JIMWLK evolution equations. The quadrupole amplitude evolution equation was derived in the large- N_c limit in [63], and beyond the large- N_c limit in [65]. Again, Eq. (38) is valid only as long as the rapidities y_1 and y_2 of the two produced gluons are close to each other, $|y_2 - y_1| \lesssim 1/\alpha_s$, such that no small- x evolution corrections need to be included in the $[y_1, y_2]$ rapidity interval.

E. Two-gluon production with long-range rapidity correlations: the net result

Equations (33) and (38), when combined, give us the two-gluon production cross section in the heavy-light ion collisions:

$$\frac{d\sigma}{d^2k_1 dy_1 d^2k_2 dy_2} = \frac{d\sigma_{square}}{d^2k_1 dy_1 d^2k_2 dy_2} + \frac{d\sigma_{crossed}}{d^2k_1 dy_1 d^2k_2 dy_2}. \tag{39}$$

This production cross section is the main formal result of this work. We analyze the properties of the cross section (39) below.

IV. LONG-RANGE RAPIDITY CORRELATIONS: AWAY-SIDE AND NEAR-SIDE; HBT CORRELATIONS

Our goal now is to evaluate the correlations resulting from the two-gluon production cross section (39), that is from the cross sections in Eqs. (33) and (38). The first step is to evaluate the interaction with the target. We will be working in the quasi-classical MV/GM limit, where the interaction and, hence, the production cross sections (33) and (38), are rapidity-independent.

We begin with the cross section in Eq. (33). Even in the quasi-classical limit, evaluation of the interaction in Eq. (31) is computationally intensive (though conceptually rather straightforward). To simplify the calculation we will also employ the large- N_c expansion: we assume that the nucleons in the nuclei are made out of an order- N_c^2 valence quarks (or gluons), such that the saturation scale, which in such case is proportional to $Q_{s0}^2 \sim \alpha_s^2 N_c^2$, is constant in the 't Hooft's large- N_c limit. In the saturation physics framework such approximation was used in [63] for the quadrupole operator giving a reasonably good approximation to the exact answer [66]. Similar approximations are frequently used (albeit, often implicitly) in applications of anti-de Sitter space/conformal field theory (AdS/CFT) correspondence to collisions of heavy ions modeled by shock waves [68–71].

At the leading order in $1/N_c^2$ expansion of Eq. (33) the interaction with the target factorizes, as discussed around Eq. (34). In addition, the cross section in Eq. (38) is $1/N_c^2$ -suppressed (as compared to the leading term in Eq. (33)) and can be neglected at the leading order in N_c . The correlation function is then given by Eq. (17) with the single gluon production cross section from Eq. (29). In the MV/GM approximation the gluon color dipole interaction with the target is [53]

$$S_G(\mathbf{x}_1, \mathbf{x}_2, y=0) = \exp \left[-\frac{1}{4} |\mathbf{x}_1 - \mathbf{x}_2|^2 Q_{s0}^2 \left(\frac{\mathbf{x}_1 + \mathbf{x}_2}{2} \right) \ln \left(\frac{1}{|\mathbf{x}_1 - \mathbf{x}_2| \Lambda} \right) \right] \tag{40}$$

with Q_{s0} the rapidity-independent gluon saturation scale in the quasi-classical limit evaluated at the dipole center-of-mass $(\mathbf{x}_1 + \mathbf{x}_2)/2$ and Λ an infrared (IR) cutoff. We see that the quasi-classical single gluon production cross section is rapidity-independent and, for unpolarized nuclei and for perturbatively large k_T [54], is also independent of the

azimuthal angle ϕ of the transverse momentum \mathbf{k} of the outgoing gluon. We conclude that at the leading order in $1/N_c^2$ in the quasi-classical approximation the geometric correlations are almost absent and the correlation function (17) is approximately zero.

Non-trivial correlations can be obtained from Eq. (33) by expanding the interaction term to the first non-trivial order in $1/N_c^2$. To this end we write a correlator of two Wilson line traces as

$$\frac{1}{(N_c^2 - 1)^2} \langle \text{Tr}[U_{\mathbf{x}_1} U_{\mathbf{x}_2}^\dagger] \text{Tr}[U_{\mathbf{x}_3} U_{\mathbf{x}_4}^\dagger] \rangle = \frac{1}{(N_c^2 - 1)^2} \langle \text{Tr}[U_{\mathbf{x}_1} U_{\mathbf{x}_2}^\dagger] \rangle \langle \text{Tr}[U_{\mathbf{x}_3} U_{\mathbf{x}_4}^\dagger] \rangle + \Delta(\mathbf{x}_1, \mathbf{x}_2, \mathbf{x}_3, \mathbf{x}_4), \quad (41)$$

where the correction to the factorized expression (34), denoted by Δ , is order- $1/N_c^2$. (Note that each adjoint trace in Eq. (41) is order- $(N_c^2 - 1)$, such that its left-hand side, as well as the first term on its right-hand side, are order-one in N_c counting.)

The leading order- $1/N_c^2$ contribution to Δ is derived in the Appendix, with the result being

$$\Delta(\mathbf{x}_1, \mathbf{x}_2, \mathbf{x}_3, \mathbf{x}_4) = \frac{(D_3 - D_2)^2}{N_c^2} \left[\frac{e^{D_1}}{D_1 - D_2} - \frac{2e^{D_1}}{(D_1 - D_2)^2} + \frac{e^{D_1}}{D_1 - D_3} - \frac{2e^{D_1}}{(D_1 - D_3)^2} \right. \\ \left. + \frac{2e^{\frac{1}{2}(D_1 + D_2)}}{(D_1 - D_2)^2} + \frac{2e^{\frac{1}{2}(D_1 + D_3)}}{(D_1 - D_3)^2} \right] + O\left(\frac{1}{N_c^4}\right), \quad (42)$$

where we have defined

$$D_1 = -\frac{Q_{s0}^2}{4} \left[|\mathbf{x}_1 - \mathbf{x}_2|^2 \ln \left(\frac{1}{|\mathbf{x}_1 - \mathbf{x}_2| \Lambda} \right) + |\mathbf{x}_3 - \mathbf{x}_4|^2 \ln \left(\frac{1}{|\mathbf{x}_3 - \mathbf{x}_4| \Lambda} \right) \right] \quad (43a)$$

$$D_2 = -\frac{Q_{s0}^2}{4} \left[|\mathbf{x}_1 - \mathbf{x}_3|^2 \ln \left(\frac{1}{|\mathbf{x}_1 - \mathbf{x}_3| \Lambda} \right) + |\mathbf{x}_2 - \mathbf{x}_4|^2 \ln \left(\frac{1}{|\mathbf{x}_2 - \mathbf{x}_4| \Lambda} \right) \right] \quad (43b)$$

$$D_3 = -\frac{Q_{s0}^2}{4} \left[|\mathbf{x}_1 - \mathbf{x}_4|^2 \ln \left(\frac{1}{|\mathbf{x}_1 - \mathbf{x}_4| \Lambda} \right) + |\mathbf{x}_2 - \mathbf{x}_3|^2 \ln \left(\frac{1}{|\mathbf{x}_2 - \mathbf{x}_3| \Lambda} \right) \right] \quad (43c)$$

assuming, for simplicity, that all the saturation scales are evaluated at the same impact parameter.

Using Eq. (41) in Eq. (33) we see that the correlated part of the two-gluon production cross section is

$$\frac{d\sigma_{square}^{(corr)}}{d^2k_1 dy_1 d^2k_2 dy_2} = \frac{\alpha_s^2 C_F^2}{16\pi^8} \int d^2B d^2b_1 d^2b_2 T_1(\mathbf{B} - \mathbf{b}_1) T_1(\mathbf{B} - \mathbf{b}_2) d^2x_1 d^2y_1 d^2x_2 d^2y_2 e^{-i\mathbf{k}_1 \cdot (\mathbf{x}_1 - \mathbf{y}_1) - i\mathbf{k}_2 \cdot (\mathbf{x}_2 - \mathbf{y}_2)} \\ \times \frac{\mathbf{x}_1 - \mathbf{b}_1}{|\mathbf{x}_1 - \mathbf{b}_1|^2} \cdot \frac{\mathbf{y}_1 - \mathbf{b}_1}{|\mathbf{y}_1 - \mathbf{b}_1|^2} \frac{\mathbf{x}_2 - \mathbf{b}_2}{|\mathbf{x}_2 - \mathbf{b}_2|^2} \cdot \frac{\mathbf{y}_2 - \mathbf{b}_2}{|\mathbf{y}_2 - \mathbf{b}_2|^2} \\ \times [\Delta(\mathbf{x}_1, \mathbf{y}_1, \mathbf{x}_2, \mathbf{y}_2) - \Delta(\mathbf{x}_1, \mathbf{y}_1, \mathbf{x}_2, \mathbf{b}_2) - \Delta(\mathbf{x}_1, \mathbf{y}_1, \mathbf{b}_2, \mathbf{y}_2) - \Delta(\mathbf{x}_1, \mathbf{b}_1, \mathbf{x}_2, \mathbf{y}_2) - \Delta(\mathbf{b}_1, \mathbf{y}_1, \mathbf{x}_2, \mathbf{y}_2) \\ + \Delta(\mathbf{x}_1, \mathbf{b}_1, \mathbf{x}_2, \mathbf{b}_2) + \Delta(\mathbf{x}_1, \mathbf{b}_1, \mathbf{b}_2, \mathbf{y}_2) + \Delta(\mathbf{b}_1, \mathbf{y}_1, \mathbf{x}_2, \mathbf{b}_2) + \Delta(\mathbf{b}_1, \mathbf{y}_1, \mathbf{b}_2, \mathbf{y}_2)]. \quad (44)$$

Eq. (44) along with the expression for Δ in Eq. (42) are our most complete results for the contribution to the two-gluon production cross section coming from Eq. (33) in the quasi-classical regime of the heavy-light ion collisions in the large- N_c limit. The evaluation of the full Eq. (44) appears to be rather involved and is left for the future work.

Instead we will expand Eq. (42) and use the result in Eq. (44) to obtain the correlated gluon production at the lowest non-trivial order. This result can be used to elucidate the structure of the long-range rapidity correlations, along with the comparison to the existing expressions in the literature.

At the lowest non-trivial order in D_i 's (that is, since each D_i represents a two-gluon exchange with the target, at the lowest order in the number of gluon exchanges corresponding to $k_{1T}, k_{2T} \gg Q_{s0}$), Eq. (42) becomes

$$\Delta(\mathbf{x}_1, \mathbf{x}_2, \mathbf{x}_3, \mathbf{x}_4) \approx \frac{(D_3 - D_2)^2}{2N_c^2}. \quad (45)$$

Substituting this into Eq. (44) we can further simplify the expression by assuming that for the connected diagrams that contribute to the Δ 's one has \mathbf{b}_1 and \mathbf{b}_2 perturbatively close to each other, with the typical separation between these two impact parameters much smaller than the nucleon radius. Since the nuclear profile functions for a large nucleus do not vary much over perturbatively short distances we can put $\mathbf{b}_1 \approx \mathbf{b}_2 \approx \mathbf{b}$ in the arguments of T_1 's and Q_{s0} , where $\mathbf{b} \equiv (\mathbf{b}_1 + \mathbf{b}_2)/2$. Defining $\Delta\mathbf{b} \equiv \mathbf{b}_1 - \mathbf{b}_2$ we can write $d^2b_1 d^2b_2 = d^2b d^2\Delta\mathbf{b}$. The integral over $\Delta\mathbf{b}$ can be then carried out with the help of a Fourier transform

$$\frac{1}{4} |\mathbf{x}|^2 \ln \left(\frac{1}{|\mathbf{x}| \Lambda} \right) = \int \frac{d^2l}{2\pi} (1 - e^{i\mathbf{l} \cdot \mathbf{x}}) \frac{1}{(l^2)^2} \quad (46)$$

used to replace $(D_3 - D_2)^2$ in Eq. (45) and, hence, all Δ 's in Eq. (44) as a double Fourier-integral: for instance

$$\begin{aligned}\Delta(\mathbf{x}_1, \mathbf{y}_1, \mathbf{x}_2, \mathbf{y}_2) &= \frac{Q_{s0}^4}{2N_c^2} \int \frac{d^2l d^2l'}{(2\pi)^2} \frac{1}{(l^2)^2} \frac{1}{(l'^2)^2} \left[e^{i\mathbf{l} \cdot (\mathbf{x}_1 - \mathbf{x}_2)} + e^{i\mathbf{l} \cdot (\mathbf{y}_1 - \mathbf{y}_2)} - e^{i\mathbf{l} \cdot (\mathbf{x}_1 - \mathbf{y}_2)} - e^{i\mathbf{l} \cdot (\mathbf{y}_1 - \mathbf{x}_2)} \right] \\ &\quad \times \left[e^{-i\mathbf{l}' \cdot (\mathbf{x}_1 - \mathbf{x}_2)} + e^{-i\mathbf{l}' \cdot (\mathbf{y}_1 - \mathbf{y}_2)} - e^{-i\mathbf{l}' \cdot (\mathbf{x}_1 - \mathbf{y}_2)} - e^{-i\mathbf{l}' \cdot (\mathbf{y}_1 - \mathbf{x}_2)} \right] \\ &= \frac{Q_{s0}^4}{2N_c^2} \int \frac{d^2l d^2l'}{(2\pi)^2} \frac{1}{(l^2)^2} \frac{1}{(l'^2)^2} \left[e^{i\mathbf{l} \cdot (\tilde{\mathbf{x}}_1 - \tilde{\mathbf{x}}_2)} + e^{i\mathbf{l} \cdot (\tilde{\mathbf{y}}_1 - \tilde{\mathbf{y}}_2)} - e^{i\mathbf{l} \cdot (\tilde{\mathbf{x}}_1 - \tilde{\mathbf{y}}_2)} - e^{i\mathbf{l} \cdot (\tilde{\mathbf{y}}_1 - \tilde{\mathbf{x}}_2)} \right] \\ &\quad \times \left[e^{-i\mathbf{l}' \cdot (\tilde{\mathbf{x}}_1 - \tilde{\mathbf{x}}_2)} + e^{-i\mathbf{l}' \cdot (\tilde{\mathbf{y}}_1 - \tilde{\mathbf{y}}_2)} - e^{-i\mathbf{l}' \cdot (\tilde{\mathbf{x}}_1 - \tilde{\mathbf{y}}_2)} - e^{-i\mathbf{l}' \cdot (\tilde{\mathbf{y}}_1 - \tilde{\mathbf{x}}_2)} \right] e^{i(\mathbf{l} - \mathbf{l}') \cdot \Delta \mathbf{b}}\end{aligned}\quad (47)$$

where we employed the substitution

$$\tilde{\mathbf{x}}_1 = \mathbf{x}_1 - \mathbf{b}_1, \quad \tilde{\mathbf{y}}_1 = \mathbf{y}_1 - \mathbf{b}_1, \quad \tilde{\mathbf{x}}_2 = \mathbf{x}_2 - \mathbf{b}_2, \quad \tilde{\mathbf{y}}_2 = \mathbf{y}_2 - \mathbf{b}_2. \quad (48)$$

Performing similar substitutions for all Δ 's in Eq. (44), we can integrate over $\Delta \mathbf{b}$, $\tilde{\mathbf{x}}_1$, $\tilde{\mathbf{x}}_2$, $\tilde{\mathbf{y}}_1$, $\tilde{\mathbf{y}}_2$, and \mathbf{l}' . After some algebra one arrives at (cf. [11, 12])

$$\left. \frac{d\sigma_{square}^{(corr)}}{d^2k_1 dy_1 d^2k_2 dy_2} \right|_{LO} = \frac{\alpha_s^2}{4\pi^4} \int d^2B d^2b [T_1(\mathbf{B} - \mathbf{b})]^2 \frac{Q_{s0}^4(\mathbf{b})}{\mathbf{k}_1^2 \mathbf{k}_2^2} \int_{\Lambda} \frac{d^2l}{(l^2)^2} \left[\frac{1}{(\mathbf{k}_1 - \mathbf{l})^2 (\mathbf{k}_2 + \mathbf{l})^2} + \frac{1}{(\mathbf{k}_1 - \mathbf{l})^2 (\mathbf{k}_2 - \mathbf{l})^2} \right], \quad (49)$$

where the subscript *LO* denotes the lowest-order cross section.

Equation (49) is illustrated in Fig. 8 by regular Feynman diagrams that contribute to its right-hand-side (cf. [11, 12]): these diagrams are referred to as the “glasma” graphs in the literature. The momenta of the gluon lines are labeled in Fig. 8, and the triple gluon vertices, marked by the dark circles, are the effective Lipatov vertices. These particular graphs contribute to the first and the second terms in the square brackets of Eq. (49) correspondingly, and can be calculated by taking two Lipatov vertices squared.

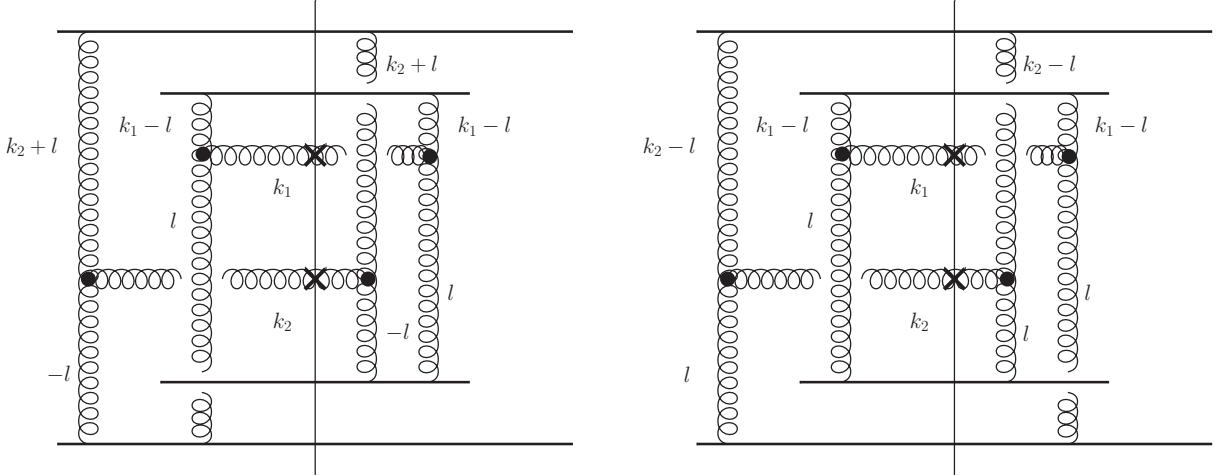


FIG. 8. Examples of diagrams generating contributions to Eq. (49): the left panel represent the away-side correlations (the first term in Eq. (49)), while the right panel contributes near-side correlations (the second term in Eq. (49)). The t -channel gluon momenta flow toward the triple-gluon vertices to the left of the cut, and away from those vertices to the right of the cut.

The obtained expression (49) contains both the near-side and away-side azimuthal correlations [11, 12]: clearly the first term in the square brackets of Eq. (49) contains poles at $\mathbf{l} = \mathbf{k}_1$ and $\mathbf{l} = -\mathbf{k}_2$, which, after integration over l , lead to a contribution²

$$\sim \frac{1}{(\mathbf{k}_1 + \mathbf{k}_2)^2}, \quad (50)$$

² Note that both terms in Eq. (49) also contain a pole at $\mathbf{l} = 0$, which leads to a correlated contribution independent of the azimuthal angle between \mathbf{k}_1 and \mathbf{k}_2 .

characteristic of the away-side correlations.

The second term in the square brackets of Eq. (49) has poles at $\mathbf{l} = \mathbf{k}_1$ and $\mathbf{l} = \mathbf{k}_2$, yielding a contribution

$$\sim \frac{1}{(\mathbf{k}_1 - \mathbf{k}_2)^2}, \quad (51)$$

indicating near-side correlations. Note that all correlations are long-range in rapidity since the cross section (49) is rapidity-independent.

Now we turn our attention to Eq. (38). There the cross section contribution itself is $1/N_c^2$ -suppressed as compared to the leading (uncorrelated) part of Eq. (33): hence we need to evaluate the interaction with the target in (38) using the large- N_c limit. We work in the same quasi-classical MV/GM approximation, along with the large- N_c limit. The fundamental (quark) quadrupole amplitude was evaluated in this approximation in [63] (see Eq. (14) there), yielding

$$Q_{quark}(\mathbf{x}_1, \mathbf{x}_2, \mathbf{x}_3, \mathbf{x}_4) = e^{D_1/2} + \frac{D_3 - D_2}{D_1 - D_3} \left[e^{D_1/2} - e^{D_3/2} \right]. \quad (52)$$

Since the adjoint (gluon) quadrupole (36) in the large- N_c limit is simply

$$Q(\mathbf{x}_1, \mathbf{x}_2, \mathbf{x}_3, \mathbf{x}_4) = [Q_{quark}(\mathbf{x}_1, \mathbf{x}_2, \mathbf{x}_3, \mathbf{x}_4)]^2 \quad (53)$$

we get

$$Q(\mathbf{x}_1, \mathbf{x}_2, \mathbf{x}_3, \mathbf{x}_4) = \left[e^{D_1/2} + \frac{D_3 - D_2}{D_1 - D_3} \left(e^{D_1/2} - e^{D_3/2} \right) \right]^2. \quad (54)$$

Equations (54) and (40), when used in Eq. (38), give us the remaining contribution to the two-gluon production cross section in the quasi-classical approximation, which has to be added to Eq. (44).

Again the full expression (38) is hard to evaluate: instead, similar to Eq. (49), we will consider the limit of large $k_{1T} = |\mathbf{k}_1|$ and $k_{2T} = |\mathbf{k}_2|$: $k_1, k_2 \gg Q_{s0}$. Expanding Eq. (54) in the powers of D_i 's yields

$$Q(\mathbf{x}_1, \mathbf{x}_2, \mathbf{x}_3, \mathbf{x}_4) = 1 + D_1 - D_2 + D_3 + \frac{1}{4} [2 D_1^2 + D_2^2 + 2 D_3^2 - 3 D_1 D_2 - 3 D_2 D_3 + 3 D_1 D_3] + O(D_i^3). \quad (55)$$

Using this result along with a similar expansion for Eq. (40) in Eq. (37), and employing again the Fourier transform (46) along with the substitution (48) one can write

$$\begin{aligned} Int_{crossed}(\mathbf{x}_1, \mathbf{y}_1, \mathbf{b}_1, \mathbf{x}_2, \mathbf{y}_2, \mathbf{b}_2) = Q_{s0}^4 \int \frac{d^2 l d^2 l'}{(2\pi)^2} \frac{1}{(l^2)^2} \frac{1}{(l'^2)^2} \left\{ e^{i(l-l') \cdot \Delta \mathbf{b}} \left(1 - e^{i \mathbf{l}' \cdot \tilde{\mathbf{x}}_2} \right) \left(1 - e^{-i \mathbf{l} \cdot \tilde{\mathbf{y}}_2} \right) \right. \\ \times \left[\frac{1}{2} \left(1 - e^{-i \mathbf{l}' \cdot \tilde{\mathbf{x}}_1} \right) \left(1 - e^{i \mathbf{l} \cdot \tilde{\mathbf{y}}_1} \right) + \left(1 - e^{i \mathbf{l} \cdot \tilde{\mathbf{x}}_1} \right) \left(1 - e^{-i \mathbf{l}' \cdot \tilde{\mathbf{y}}_1} \right) \right] \\ \left. + \left(1 - e^{i \mathbf{l} \cdot \tilde{\mathbf{x}}_1} \right) \left(1 - e^{-i \mathbf{l}' \cdot \tilde{\mathbf{x}}_2} \right) \left(1 - e^{-i \mathbf{l} \cdot \tilde{\mathbf{y}}_1} \right) \left(1 - e^{i \mathbf{l}' \cdot \tilde{\mathbf{y}}_2} \right) \right\} \end{aligned} \quad (56)$$

where the $\mathbf{l} \leftrightarrow \mathbf{l}'$, $\mathbf{l} \leftrightarrow -\mathbf{l}$, and $\mathbf{l}' \leftrightarrow -\mathbf{l}'$ symmetries of the integrand were utilized to cast the expression in its present form. Using Eq. (56) to replace the interaction with the target in Eq. (38) and integrating over $\tilde{\mathbf{x}}_1$, $\tilde{\mathbf{x}}_2$, $\tilde{\mathbf{y}}_1$, $\tilde{\mathbf{y}}_2$, and, in some terms, over \mathbf{l}' , leads to the following result

$$\left. \frac{d\sigma_{crossed}}{d^2 k_1 dy_1 d^2 k_2 dy_2} \right|_{LO} = \left. \frac{d\sigma_{crossed}^{(corr)}}{d^2 k_1 dy_1 d^2 k_2 dy_2} \right|_{LO} + \left. \frac{d\sigma_{HBT}}{d^2 k_1 dy_1 d^2 k_2 dy_2} \right|_{LO} \quad (57)$$

where

$$\begin{aligned} \left. \frac{d\sigma_{crossed}^{(corr)}}{d^2 k_1 dy_1 d^2 k_2 dy_2} \right|_{LO} = \frac{\alpha_s^2}{32 \pi^4} \int d^2 B d^2 b [T_1(\mathbf{B} - \mathbf{b})]^2 \frac{Q_{s0}^4(\mathbf{b})}{\mathbf{k}_1^2 \mathbf{k}_2^2} \int \frac{d^2 l}{(l^2)^2 ((\mathbf{l} - \mathbf{k}_1 + \mathbf{k}_2)^2)^2 ((\mathbf{k}_1 - \mathbf{l})^2)^2 ((\mathbf{k}_2 + \mathbf{l})^2)^2} \\ \times \{ [l^2 (\mathbf{k}_2 + \mathbf{l})^2 + (\mathbf{k}_1 - \mathbf{l})^2 (\mathbf{l} - \mathbf{k}_1 + \mathbf{k}_2)^2 - \mathbf{k}_1^2 (\mathbf{k}_2 - \mathbf{k}_1 + 2\mathbf{l})^2] \\ \times [l^2 (\mathbf{k}_1 - \mathbf{l})^2 + (\mathbf{k}_2 + \mathbf{l})^2 (\mathbf{l} - \mathbf{k}_1 + \mathbf{k}_2)^2 - \mathbf{k}_2^2 (\mathbf{k}_2 - \mathbf{k}_1 + 2\mathbf{l})^2] \\ + 4 l^2 (\mathbf{l} - \mathbf{k}_1 + \mathbf{k}_2)^2 [((\mathbf{k}_1 - \mathbf{l})^2)^2 + ((\mathbf{k}_2 + \mathbf{l})^2)^2] \} + (\mathbf{k}_2 \rightarrow -\mathbf{k}_2) \end{aligned} \quad (58)$$

and

$$\begin{aligned} \left. \frac{d\sigma_{HBT}}{d^2k_1 dy_1 d^2k_2 dy_2} \right|_{LO} &= \frac{\alpha_s^2}{16\pi^4} \int d^2B d^2b [T_1(\mathbf{B} - \mathbf{b})]^2 \frac{Q_{s0}^4(\mathbf{b})}{\mathbf{k}_1^2 \mathbf{k}_2^2} [\delta^2(\mathbf{k}_1 - \mathbf{k}_2) + \delta^2(\mathbf{k}_1 + \mathbf{k}_2)] \\ &\times \int_{\Lambda} \frac{d^2l d^2l'}{(\mathbf{l}^2)^2 (\mathbf{l}'^2)^2 ((\mathbf{k}_1 - \mathbf{l})^2 ((\mathbf{k}_1 + \mathbf{l}')^2)^2} \left[\mathbf{l}^2 (\mathbf{k}_1 + \mathbf{l}')^2 + \mathbf{l}'^2 (\mathbf{k}_1 - \mathbf{l})^2 - \mathbf{k}_1^2 (\mathbf{l} + \mathbf{l}')^2 \right]^2. \end{aligned} \quad (59)$$

We will explain the origin of the ‘‘HBT’’ label on the cross section in Eq. (59) in a little while below: we defer the analysis of Eq. (59) until then.

First we concentrate on the expression (58). We note that by shifting the integration momentum \mathbf{l} one could reduce the second term in the curly brackets (together with the $\mathbf{k}_2 \rightarrow -\mathbf{k}_2$ term) to that in Eq. (49), thus doubling Eq. (49). That term is still described by the diagrams of the type shown in Fig. 8 and gives the near- and away-side correlations in Eqs. (50) and (51).

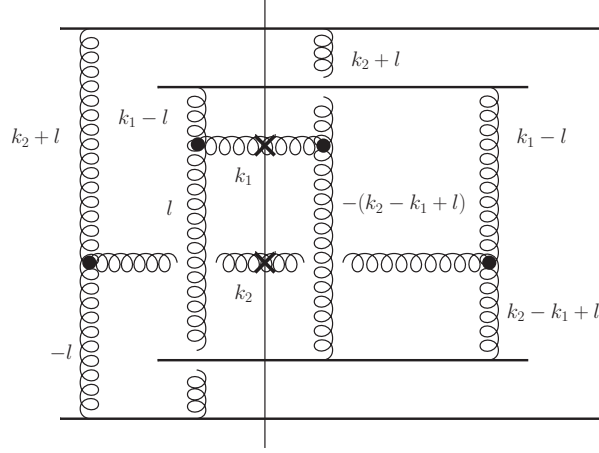


FIG. 9. An example of a diagram giving a contribution to the first term in the curly brackets of Eq. (58).

The first term in the curly brackets of Eq. (58) corresponds to a different class of diagrams, one of which is shown in Fig. 9. One can see that the diagram in Fig. 9 contributes two non-forward ‘‘squares’’ of the effective Lipatov vertices. An analysis of the poles of the integral in the first term of Eq. (58) shows that it contains similar near- and away-side correlations to that in Eqs. (50) and (51), though with an additional enhancement due to a prefactor,

$$\sim [2(\mathbf{k}_1 \cdot \mathbf{k}_2)^2 - \mathbf{k}_1^2 \mathbf{k}_2^2] \left[\frac{1}{(\mathbf{k}_1 - \mathbf{k}_2)^2} + \frac{1}{(\mathbf{k}_1 + \mathbf{k}_2)^2} \right]. \quad (60)$$

The origin of this contribution to correlations is in the non-forward squares of the Lipatov vertices, which is similar to the mechanism for generating long-range rapidity correlations proposed in [39] using two BFKL ladders with non-zero momentum transfer. Note, however, that we do not obtain the correlation proportional to the first power of $\mathbf{k}_1 \cdot \mathbf{k}_2$ advocated in [39], perhaps due to the lowest-order nature of the result (58). It appears that the correlations (60) resulting from the lowest-order diagrams like the one depicted in Fig. 9 have not been considered in the literature yet.

Note that the away- and the near-side correlations enter Eqs. (49) and (58) on equal footing: in fact, one could be obtained from another by a simple $\mathbf{k}_2 \rightarrow -\mathbf{k}_2$ substitution in either of those expressions. While evaluating the integrals over \mathbf{l} in Eqs. (49) and (58) analytically appears to be rather algebra-intensive, we do not need to do this to observe that, once the \mathbf{l} -integral is carried out for one of the terms in the square brackets of Eq. (49), the answer for the other term is obtained by substituting $\mathbf{k}_2 \rightarrow -\mathbf{k}_2$ in the result. Equation (58) simply contains an additive $\mathbf{k}_2 \rightarrow -\mathbf{k}_2$ term.

Since the correlated cross sections (49) and (58) are sums of two terms related by the $\mathbf{k}_2 \rightarrow -\mathbf{k}_2$ substitution and are symmetric under the $\mathbf{k}_1 \leftrightarrow \mathbf{k}_2$ interchange, we conclude that they are functions only of even powers of \mathbf{k}_1 and \mathbf{k}_2 , that is functions of \mathbf{k}_1^2 , \mathbf{k}_2^2 , $(\mathbf{k}_1 \cdot \mathbf{k}_2)^2$, and possibly $(\mathbf{k}_1 \times \mathbf{k}_2)^2$. Clearly this implies that the Fourier series representation of Eqs. (49) and (58) would only contain even cosine harmonics of the azimuthal angle, that is

$$\left. \frac{d\sigma^{(corr)}}{d^2k_1 dy_1 d^2k_2 dy_2} \right|_{LO} \equiv \left. \frac{d\sigma_{square}^{(corr)}}{d^2k_1 dy_1 d^2k_2 dy_2} \right|_{LO} + \left. \frac{d\sigma_{crossed}^{(corr)}}{d^2k_1 dy_1 d^2k_2 dy_2} \right|_{LO} \sim \sum_{n=0}^{\infty} c_n(k_{1T}, k_{2T}) \cos(2n \Delta\phi) \quad (61)$$

where $\Delta\phi = \phi_1 - \phi_2$ is the angle between momenta \mathbf{k}_1 and \mathbf{k}_2 while $k_{1T} = |\mathbf{k}_1|$ and $k_{2T} = |\mathbf{k}_2|$. Here $c_n(k_1, k_2)$ are some coefficient to be determined by an exact calculation. It is quite interesting that only even harmonics contribute to the correlated cross section in Eq. (61). Let us stress here that we have not made any assumptions about the centrality of the collision: we do not have an almond-shaped overlap of the two nuclei. In fact we integrate over all impact parameters \mathbf{B} . (Also the impact parameter dependence factorizes from the rest of the expression.) Hence the correlation in Eq. (61) is not caused by the geometry of the collision.

To construct the correlation function one has to use Eqs. (49) and (58) in Eq. (15). In the latter, the uncorrelated two-gluon production would dominate in the denominator of the normalization factor, that is, in the denominator of the first factor on its right-hand side. The single-gluon production cross-section (29) at the lowest order is equal to (see [16] and references therein)

$$\left\langle \frac{d\sigma^{pA_2}}{d^2k dy d^2b} \right\rangle = \frac{\alpha_s C_F}{\pi^2} \frac{Q_{s0}^2(\mathbf{b})}{k_T^4} \ln \frac{k_T^2}{\Lambda^2}. \quad (62)$$

Using this along with the sum of Eqs. (49) and (58) in Eq. (15) and taking the large- N_c limit in Eq. (62) we get

$$\begin{aligned} C(\mathbf{k}_1, y_1, \mathbf{k}_2, y_2)|_{LO} &= \frac{1}{N_c^2} \frac{\int d^2B d^2b [T_1(\mathbf{B} - \mathbf{b})]^2 Q_{s0}^4(\mathbf{b})}{\int d^2B d^2b_1 d^2b_2 T_1(\mathbf{B} - \mathbf{b}_1) T_1(\mathbf{B} - \mathbf{b}_2) Q_{s0}^2(\mathbf{b}_1) Q_{s0}^2(\mathbf{b}_2)} \\ &\times \frac{k_1^2 k_2^2}{\ln \frac{k_1^2}{\Lambda^2} \ln \frac{k_2^2}{\Lambda^2}} \left\{ 2 \int_{\Lambda} \frac{d^2l}{(l^2)^2} \left[\frac{1}{(\mathbf{k}_1 - \mathbf{l})^2 (\mathbf{k}_2 + \mathbf{l})^2} + \frac{1}{(\mathbf{k}_1 - \mathbf{l})^2 (\mathbf{k}_2 - \mathbf{l})^2} \right] \right. \\ &+ \frac{1}{8} \left[\int \frac{d^2l}{(l^2)^2 ((\mathbf{l} - \mathbf{k}_1 + \mathbf{k}_2)^2)^2 ((\mathbf{k}_1 - \mathbf{l})^2)^2 ((\mathbf{k}_2 + \mathbf{l})^2)^2} [l^2 (\mathbf{k}_2 + \mathbf{l})^2 + (\mathbf{k}_1 - \mathbf{l})^2 (\mathbf{l} - \mathbf{k}_1 + \mathbf{k}_2)^2 - k_1^2 (\mathbf{k}_2 - \mathbf{k}_1 + 2\mathbf{l})^2] \right. \\ &\times [l^2 (\mathbf{k}_1 - \mathbf{l})^2 + (\mathbf{k}_2 + \mathbf{l})^2 (\mathbf{l} - \mathbf{k}_1 + \mathbf{k}_2)^2 - k_2^2 (\mathbf{k}_2 - \mathbf{k}_1 + 2\mathbf{l})^2] + (\mathbf{k}_2 \rightarrow -\mathbf{k}_2) \left. \right] \left. \right\}. \quad (63) \end{aligned}$$

To evaluate this further let us assume for a moment that both colliding nuclei are simply cylinders oriented along the collision axis, such that the nuclear profile functions of the nuclei are $T_i(\mathbf{b}) = 2\rho R_i \theta(R_i - b)$ where $i = 1, 2$ labels the nuclei, ρ is the (constant) nucleon number density in the nucleus, R_1 and R_2 are the radii of the projectile and target nuclei, and the cylindrical nucleus is assumed to have length $2R_i$ along its axis. Assuming that both nuclei are large and neglecting the edge effects, we can neglect the \mathbf{b}_1 and \mathbf{b}_2 dependence in these nuclear profile functions of both nuclei. Since the gluon saturation scale in the MV model is $Q_{s0}^2 = 4\pi\alpha_s^2 T_2(\mathbf{b})$ we obtain in the $R_1 \ll R_2$ limit

$$\begin{aligned} C(\mathbf{k}_1, y_1, \mathbf{k}_2, y_2)|_{LO} &= \frac{1}{N_c^2 \pi R_1^2} \frac{k_1^2 k_2^2}{\ln \frac{k_1^2}{\Lambda^2} \ln \frac{k_2^2}{\Lambda^2}} \left\{ 2 \int_{\Lambda} \frac{d^2l}{(l^2)^2} \left[\frac{1}{(\mathbf{k}_1 - \mathbf{l})^2 (\mathbf{k}_2 + \mathbf{l})^2} + \frac{1}{(\mathbf{k}_1 - \mathbf{l})^2 (\mathbf{k}_2 - \mathbf{l})^2} \right] \right. \\ &+ \frac{1}{8} \left[\int \frac{d^2l}{(l^2)^2 ((\mathbf{l} - \mathbf{k}_1 + \mathbf{k}_2)^2)^2 ((\mathbf{k}_1 - \mathbf{l})^2)^2 ((\mathbf{k}_2 + \mathbf{l})^2)^2} [l^2 (\mathbf{k}_2 + \mathbf{l})^2 + (\mathbf{k}_1 - \mathbf{l})^2 (\mathbf{l} - \mathbf{k}_1 + \mathbf{k}_2)^2 - k_1^2 (\mathbf{k}_2 - \mathbf{k}_1 + 2\mathbf{l})^2] \right. \\ &\times [l^2 (\mathbf{k}_1 - \mathbf{l})^2 + (\mathbf{k}_2 + \mathbf{l})^2 (\mathbf{l} - \mathbf{k}_1 + \mathbf{k}_2)^2 - k_2^2 (\mathbf{k}_2 - \mathbf{k}_1 + 2\mathbf{l})^2] + (\mathbf{k}_2 \rightarrow -\mathbf{k}_2) \left. \right] \left. \right\}. \quad (64) \end{aligned}$$

Indeed the correlator is suppressed by a power of N_c^2 and a power of the cross sectional area of the projectile nucleus πR_1^2 , as discussed in the literature [11–14, 40].

While our conclusion about the correlator (64) and the cross section Eq. (61) contributing only to even Fourier harmonics has been verified above at the lowest order only, it is true for the full two-gluon production cross section in heavy-light ion collisions (39). This can be seen by noticing that $\mathbf{k}_2 \rightarrow -\mathbf{k}_2$ substitution in Eq. (44) does not change the cross section, as it is equivalent to the $\mathbf{x}_2 \leftrightarrow \mathbf{y}_2$ interchange of the integration variables. The integrand of Eq. (44) (or, equivalently, of Eq. (33)) is invariant under $\mathbf{x}_2 \leftrightarrow \mathbf{y}_2$ interchange since the gluon is its own anti-particle such that $Tr[U_{\mathbf{x}} U_{\mathbf{y}}^\dagger] = Tr[U_{\mathbf{y}} U_{\mathbf{x}}^\dagger]$. The expression in Eq. (58) is explicitly invariant under $\mathbf{k}_2 \rightarrow -\mathbf{k}_2$ substitution. Hence the net correlated cross section (39) is an even function of \mathbf{k}_2 . Note also that Eqs. (33) and (38) are $\mathbf{k}_1 \leftrightarrow \mathbf{k}_2$ -symmetric: in Eq. (33) and in the term arising from the first exponential in Eq. (38) the symmetry is a consequence of the symmetry of the integrand under the simultaneous $\mathbf{x}_1 \leftrightarrow \mathbf{x}_2$, $\mathbf{y}_1 \leftrightarrow \mathbf{y}_2$, and $\mathbf{b}_1 \leftrightarrow \mathbf{b}_2$ interchanges. The term multiplying the second exponential in Eq. (38) is $\mathbf{k}_1 \leftrightarrow \mathbf{k}_2$ -symmetric due to the $\mathbf{x}_1 \leftrightarrow \mathbf{y}_1$, $\mathbf{x}_2 \leftrightarrow \mathbf{y}_2$ symmetry of the integrand, which follows from the following property of the quadrupole operator: $Tr[U_{\mathbf{x}_1} U_{\mathbf{y}_1}^\dagger U_{\mathbf{x}_2} U_{\mathbf{y}_2}^\dagger] = Tr[U_{\mathbf{y}_2} U_{\mathbf{x}_2}^\dagger U_{\mathbf{y}_1} U_{\mathbf{x}_1}^\dagger]$. We see that the net cross section (39) is decomposable into a Fourier series with even harmonics only. Therefore, the correlation function in the heavy-light ion collision can be also written as an even-harmonics series

$$C(\mathbf{k}_1, y_1, \mathbf{k}_2, y_2)|_{A_2 \gg A_1 \gg 1} \sim \sum_{n=0}^{\infty} d_n(k_{1T}, k_{2T}) \cos(2n \Delta\phi) \quad (65)$$

with some coefficients d_n . This conclusion also seems to hold in the case of classical gluon fields produced in a collision of two heavy ions, as can be seen from the result of the full numerical simulation of two-gluon production in heavy ion collisions due to classical gluon field carried out in [72]. The correlators in Figs. 9 and 10 of [72] do appear to have similar-looking maxima at $\Delta\phi = 0$ and $\Delta\phi = \pi$ (within the accuracy of the numerical error bars), though a more careful analysis is needed to figure out if our conclusion is true for two colliding heavy ions.

To better visualize the correlator let us envision a toy model in which multiple rescatterings (and other saturation effects) regulate the singularities at $\mathbf{k}_1 = \pm\mathbf{k}_2$ by the saturation scale Q_{s0} in such a way that the correlator can be modeled as proportional to

$$C_{\text{toy model}}(\mathbf{k}_1, y_1, \mathbf{k}_2, y_2) \sim \frac{1}{(\mathbf{k}_1 - \mathbf{k}_2)^2 + Q_{s0}^2} + \frac{1}{(\mathbf{k}_1 + \mathbf{k}_2)^2 + Q_{s0}^2}. \quad (66)$$

This correlator is plotted in Fig. 10 using arbitrary units along the vertical axis as a function of the azimuthal angle $\Delta\phi$ between \mathbf{k}_1 and \mathbf{k}_2 for $k_1 = k_2 = Q_{s0}$. The shape illustrates what the full correlation function may look like, having identical near- and away-side correlation peaks.

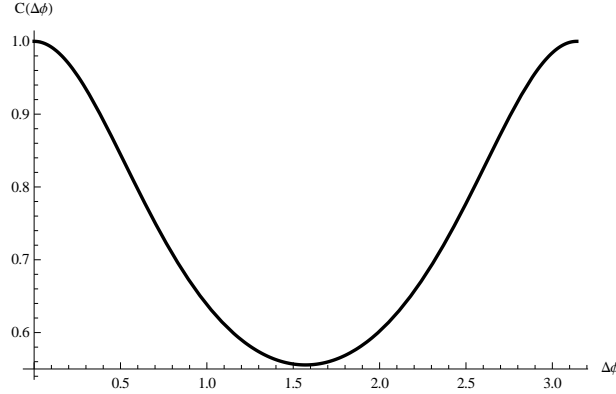


FIG. 10. A toy azimuthal two-gluon correlation function motivated by the calculation in this Section. Vertical scale is arbitrary.

Our conclusion in this Section is that the saturation/CGC dynamics in nuclear collisions appears to generate the long-range rapidity correlations which have identical maxima at both $\Delta\phi = 0$ and $\Delta\phi = \pi$ in the azimuthal angle. Such correlations are non-flow in nature, since they do not arise due to almond-shaped geometry of the collisions. (In fact the correlations should persist for the most central heavy ion collisions, though they should be suppressed by an inverse power of the overlap area as discussed above and in [11–14, 40].) However, since the elliptic flow observable v_2 (even in the reaction-plane method) is determined from two-particle correlations, it is possible that the correlations discussed here may contribute to the elliptic flow (and to higher-order even-harmonics flow observables v_{2n}) measured experimentally. It is, therefore, very important to experimentally separate our initial-state correlations from the late-time QGP effects.

Naturally the cumulant analysis [73, 74] is likely to remove these two-particle non-flow correlations from the flow observables. However, the effectiveness of the cumulant method may again depend on the collision geometry. Let us illustrate this by considering the fourth order cumulant for elliptic flow, defined by [73, 74]

$$c_2\{4\} \equiv \left\langle e^{2i(\phi_1 + \phi_2 - \phi_3 - \phi_4)} \right\rangle - \left\langle e^{2i(\phi_1 - \phi_3)} \right\rangle \left\langle e^{2i(\phi_2 - \phi_4)} \right\rangle - \left\langle e^{2i(\phi_1 - \phi_4)} \right\rangle \left\langle e^{2i(\phi_2 - \phi_3)} \right\rangle \quad (67)$$

where the angle brackets denote event averages along with the averaging over all angles ϕ_1, ϕ_2, ϕ_3 , and ϕ_4 of the four particles employed in the definition. Using the lowest-order correlations employed in arriving at Eq. (63) one can straightforwardly show that the cumulant due to these correlations only is proportional to

$$c_2\{4\}|_{LO} \propto \frac{\int d^2B d^2b_1 d^2b_2 [T_1(\mathbf{B} - \mathbf{b}_1)]^2 [T_1(\mathbf{B} - \mathbf{b}_2)]^2 Q_{s0}^4(\mathbf{b}_1) Q_{s0}^4(\mathbf{b}_2)}{\int d^2B d^2b_1 d^2b_2 d^2b_3 d^2b_4 T_1(\mathbf{B} - \mathbf{b}_1) T_1(\mathbf{B} - \mathbf{b}_2) T_1(\mathbf{B} - \mathbf{b}_3) T_1(\mathbf{B} - \mathbf{b}_4) Q_{s0}^2(\mathbf{b}_1) Q_{s0}^2(\mathbf{b}_2) Q_{s0}^2(\mathbf{b}_3) Q_{s0}^2(\mathbf{b}_4)} - \left[\frac{\int d^2B d^2b [T_1(\mathbf{B} - \mathbf{b})]^2 Q_{s0}^4(\mathbf{b})}{\int d^2B d^2b_1 d^2b_2 T_1(\mathbf{B} - \mathbf{b}_1) T_1(\mathbf{B} - \mathbf{b}_2) Q_{s0}^2(\mathbf{b}_1) Q_{s0}^2(\mathbf{b}_2)} \right]^2 \quad (68)$$

if the 4-particle correlator in Eq. (67) (the correlated part of the first term on its right-hand-side) is due to the pairwise correlations of particles 1, 3 and 2, 4 or 1, 4 and 2, 3. Clearly, in the general case, $c_2\{4\}|_{LO}$ from Eq. (68)

is non-zero.³ Moreover, the fourth order cumulant would contain the azimuthal angles dependence resulting from Eq. (63) but not shown explicitly in Eq. (68). We see that the geometric correlations from Sec. II may prevent complete removal of these non-flow correlations in the cumulants. Just like with the correlator of Eq. (20), the above non-flow correlations can be completely removed from the cumulants for the fixed impact parameter \mathbf{B} : if we fix \mathbf{B} in Eq. (68) (that is, remove all the d^2B integrations from it), we get $c_2\{4\}|_{LO} = 0$, which is exactly what the cumulant is designed to do [73, 74] — completely cancel for non-flow correlations. Note that since, in the actual experimental analyses one effectively integrates over \mathbf{B} in a given centrality bin, it is possible that some non-flow correlations (63) would remain in the cumulant (68). Even fixing $|\mathbf{B}|$ precisely and integrating over the angles of \mathbf{B} may generate a non-zero contribution of these correlations to the cumulant. The question of the interplay of the true QGP flow and the non-flow correlations discussed here has to be resolved by a more detailed numerical study.

To clarify the physical meaning of the cross section obtained in Eq. (59) we again consider a collisions of cylindrical nuclei. With this simplification we can consider one of the terms in the interaction with the target, say the $Q(\mathbf{x}_1, \mathbf{y}_1, \mathbf{x}_2, \mathbf{y}_2)$ in Eq. (37). Among many terms which contribute to the quadrupole amplitude in Eq. (55), there is a term

$$Q(\mathbf{x}_1, \mathbf{y}_1, \mathbf{x}_2, \mathbf{y}_2) \Big|_{\text{order-}Q_{s0}^4} \sim (\mathbf{x}_1 - \mathbf{y}_1)^2 Q_{s0}^2 \ln \left(\frac{1}{|\mathbf{x}_1 - \mathbf{y}_1| \Lambda} \right) (\mathbf{x}_2 - \mathbf{y}_2)^2 Q_{s0}^2 \ln \left(\frac{1}{|\mathbf{x}_2 - \mathbf{y}_2| \Lambda} \right) + \dots \quad (69)$$

Using Eq. (69) in Eq. (38) and changing the interaction variables to those defined in Eq. (48) we see that the remaining \mathbf{b}_1 and \mathbf{b}_2 integrals, after shifting those variables by \mathbf{B} , become simple Fourier transforms of the projectile nucleus profile function $T_1(\mathbf{b})$,

$$\int d^2b_1 d^2b_2 T_1(\mathbf{b}_1) T_1(\mathbf{b}_2) e^{-i(\mathbf{k}_1 - \mathbf{k}_2) \cdot (\mathbf{b}_1 - \mathbf{b}_2)} + (\mathbf{k}_2 \rightarrow -\mathbf{k}_2). \quad (70)$$

In the limit of a sufficiently large projectile nucleus the Fourier transforms give a delta-function, yielding

$$\frac{d\sigma_{HBT}}{d^2k_1 dy_1 d^2k_2 dy_2} \sim \delta^2(\mathbf{k}_1 - \mathbf{k}_2) + \delta^2(\mathbf{k}_1 + \mathbf{k}_2), \quad (71)$$

in agreement with the result in Eq. (59). Our present estimate shows that a more careful evaluation of Eq. (70) would give a smother peak in $|\mathbf{k}_1 - \mathbf{k}_2|$ at $\mathbf{k}_1 = \mathbf{k}_2$ with the width determined by the inverse radius of the projectile nucleus R_1 .

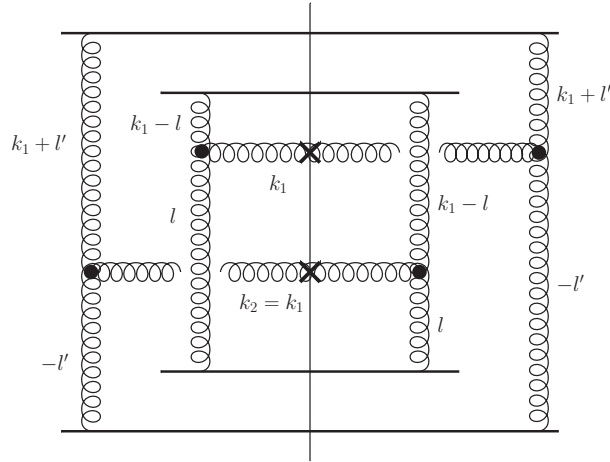


FIG. 11. An example of a lowest-order diagram generating HBT-type correlations.

The first term on the right-hand-side of Eq. (71) (or Eq. (70)) has the trademark form of the Hanbury Brown–Twiss (HBT) correlations [51], which are widely studied in heavy ion physics [75–77]. These correlations are normally local both in rapidity ($y_1 = y_2$) and in the transverse momentum $\mathbf{k}_1 = \mathbf{k}_2$: however, in Eq. (59) (or, in Eq. (71)) we only

³ Note, however, that for the heavy-light nuclear collision case considered here, $A_1 \ll A_2$, and for cylindrical nuclei, one gets $c_2\{4\}|_{LO} = 0$.

have locality in transverse momenta. This can be explained by the fact that the extent of the interaction region in the longitudinal direction, commonly labeled R_{long} , is very small in our case due to the extreme Lorentz-contraction of the two colliding nuclei leading to smearing of the longitudinal HBT correlations.

We conclude that the correlations resulting from Eq. (38) include HBT. Diagrammatic representation of the HBT correlations was discussed earlier in [78]. An example of the diagram giving rise to the correlations in Eq. (59) is shown in Fig. 11.

Interestingly though, due to the $\mathbf{k}_2 \leftrightarrow -\mathbf{k}_2$ symmetry of the two-gluon production cross section (38), the HBT peak at $\mathbf{k}_1 = \mathbf{k}_2$ in Eq. (59) is accompanied by an identical peak at $\mathbf{k}_1 = -\mathbf{k}_2$ resulting from $\delta^2(\mathbf{k}_1 + \mathbf{k}_2)$. We thus obtain a back-to-back HBT correlation resulting from multiple rescatterings in nuclei. (The origin of our back-to-back HBT correlations is different from that of the back-to-back HBT-like correlations proposed in [79, 80].)

Note that it is possible that the process of hadronization would affect the phases of the produced gluons, possibly destroying the perturbative HBT correlations of Eq. (38) and replacing them with the HBT correlations of the non-perturbative origin. The same hadronization process may also destroy the back-to-back HBT correlations from Eq. (59).

V. CONCLUSION

Above we have derived the cross section for two-gluon production in the heavy-light ion collisions. The cross section is given by Eq. (39), with the two contributions shown in Eqs. (33) and (38). Concentrating on gluon production with a long-range separation in rapidity of the two gluons we evaluated the interaction with the target in Eq. (33) using the MV/GM approximation in Eq. (42). The interaction with the target in Eq. (38) in the MV-model framework can be obtained from Eqs. (40) and (54).

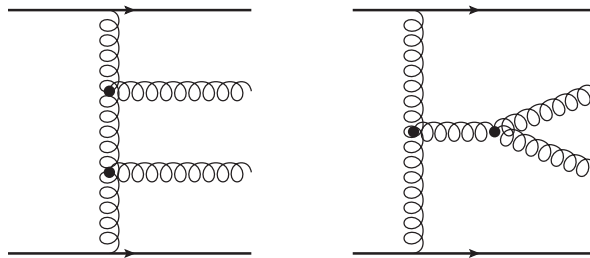


FIG. 12. Two-gluon production in a standard pQCD formalism, with the diagram on the left generating back-to-back correlations, and the diagram on the right responsible for the near-side collinear correlations.

Analyzing the corresponding correlation function we identified four main types of correlations: (i) geometric correlations, (ii) HBT correlations, (iii) away-side correlations, and (iv) the near-side correlations. HBT correlations (ii) are local in rapidity and thus are outside the main scope of our work here: however, we find that HBT correlations arising in our calculation are accompanied by a back-to-back HBT peak, as follows from Eq. (59). Geometric correlations (i) arise in Eq. (17) due to nucleons being confined within the same nucleus: more work is needed to see how strong they are and what role they are playing in experimental data.

Concentrating on the long-range rapidity correlations (iii) and (iv) we have shown that the two correlations have identical azimuthal profiles centered around $\Delta\phi = \pi$ and $\Delta\phi = 0$ correspondingly. This result is true to all orders of the calculation in the heavy-light ion collision considered here. Let us stress here the difference between this result and the regular jet correlations: indeed a two-hadron production cross section calculated in perturbative QCD (pQCD), illustrated by the examples in Fig. 12, contains both the back-to-back and near-side correlations. However, while the jet back-to-back correlations are long-range in rapidity, the jet near-side correlations are local in rapidity, being due to collinear jet showers around the trigger hadron (see [81, 82] for an analysis of mini-jet correlations in heavy ion collisions). Hence in standard pQCD formalism the strengths along with rapidity and azimuthal shapes of the back-to-back and near-side correlations are different. This is in stark contrast to our correlations (iii) and (iv), which are both long-range in rapidity, and have identical amplitudes and rapidity/azimuthal shapes. The correlations (iii) and (iv) arise due to multiple rescatterings in both nuclei and are, therefore, typical of the ion-ion collisions, weakening in the limit when one (or both) of the ions is (are) small (a proton). It is possible that this correlation would complicate the experimental extraction of the elliptic flow observable v_2 due to the QGP flow in heavy ion collisions, though it may also be that the correlation is too weak to present a significant background. More detailed numerical analysis of our result is needed to clarify this point.

ACKNOWLEDGMENTS

The authors are grateful to Adrian Dumitru, Ulrich Heinz, Jamal Jalilian-Marian, Mike Lisa, and Kirill Tuchin for inspiring discussions of two-particle correlations.

This research is sponsored in part by the U.S. Department of Energy under Grant No. DE-SC0004286.

After this paper had been posted online as a preprint, a new experimental result [83] appeared, reporting on the discovery of identical near- and away-side correlations found in the $p + Pb$ collisions at the LHC, in qualitative agreement with one of the main results of this work.

VI. APPENDIX

Our goal here is to calculate the following object

$$\frac{1}{(N_c^2 - 1)^2} \langle \text{Tr}[U_{x_1} U_{x_2}^\dagger] \text{Tr}[U_{x_3} U_{x_4}^\dagger] \rangle \quad (\text{A1})$$

in the quasi-classical MV/GM approximation at the lowest non-trivial order in $1/N_c^2$ expansion in the 't Hooft's large- N_c limit. We assume that the saturation scale is N_c -independent, that is $Q_{s0}^2 \sim (N_c)^0$, due to an order- N_c^2 number of “valence” partons in each nucleon in the target nucleus.

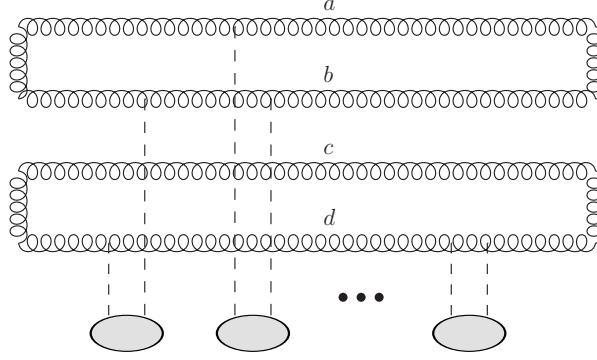


FIG. 13. Diagrams contributing to the correlator in Eq. (A1) in the quasi-classical approximation. Vertical dashed lines denote t -channel gluons, while the shaded ovals represent the nucleons in the target nucleus.

A sample of the diagrams contributing to Eq. (A1) is shown in Fig. 13, where the t -channel gluons are denoted by dashed lines to simplify the picture. The calculation is straightforward [84]: one simply has to exponentiate the two-gluon exchange interaction with a single nucleon (the nucleons are denoted by shaded ovals in Fig. 13). The only complication is that, unlike the dipole amplitude calculated in [53], the interaction now, for the double-trace operator (A1), is a matrix in the color space. A double trace operator like (A1) with the Wilson lines in the fundamental representation was calculated earlier in [85] (for similar calculations see also [65, 67, 86]).

To exponentiate the matrix we have to choose a basis in the color space of four s -channel gluons in Fig. 13: clearly the net color of the four gluons is always zero. The color states of the four gluons can be classified according to the color states of the top two s -channel gluons, since the color of the bottom pair of s -channel gluons is determined by requiring net color-neutrality of the four s -channel gluon system. The colors of a gluon pair can be decomposed in the following irreducible representations

$$\begin{aligned} (N_c^2 - 1) \otimes (N_c^2 - 1) &= V_1 \oplus V_2 \oplus V_3 \oplus V_4 \oplus V_5 \oplus V_6 \oplus V_7 \\ &= \mathbf{1} \oplus (N_c^2 - 1) \oplus \frac{N_c^2(N_c - 3)(N_c + 1)}{4} \oplus \frac{N_c^2(N_c + 3)(N_c - 1)}{4} \oplus (N_c^2 - 1) \oplus \frac{(N_c^2 - 1)(N_c^2 - 4)}{4} \oplus \frac{(N_c^2 - 1)(N_c^2 - 4)}{4}. \end{aligned} \quad (\text{A2})$$

Here we are following the notations introduced in [87], see page 120 there. Labeling the colors of the four s -channel gluons in an arbitrary color state by a, b, c , and d as shown in Fig. 13 we define the color states corresponding to

representations V_1 , V_2 , and V_5 by

$$|P_1\rangle = \frac{1}{N_c^2 - 1} \delta^{ab} \delta^{cd}, \quad |P_2\rangle = \frac{1}{\sqrt{N_c^2 - 1}} \frac{N_c}{N_c^2 - 4} d^{abe} d^{cde}, \quad |P_5\rangle = \frac{1}{\sqrt{N_c^2 - 1}} \frac{1}{N_c} f^{abe} f^{cde}, \quad (\text{A3})$$

where we differ from P_i 's in [87] by prefactors, since here we demanded that our color states are normalized to one, $\langle P_i | P_j \rangle = \delta^{ij}$. Other color states can be constructed as well [87], but we will only need the states in Eq. (A3) for the calculation below.

We denote by \hat{M} the interaction with a single nucleon by a two-gluon exchange: it is a matrix in the color space of the s -channel gluons. Since in the correlator (A1) the top (bottom) two s -channel gluons are in the color-singlet state both before and after the interaction, we write

$$\frac{1}{(N_c^2 - 1)^2} \langle \text{Tr}[U_{\mathbf{x}_1} U_{\mathbf{x}_2}^\dagger] \text{Tr}[U_{\mathbf{x}_3} U_{\mathbf{x}_4}^\dagger] \rangle = \langle P_1 | e^{\hat{M}} | P_1 \rangle. \quad (\text{A4})$$

Expanding the exponential in a power series and inserting unit operators $\mathbf{1} = \sum_i |P_i\rangle \langle P_i|$ between all the \hat{M} 's yields

$$\frac{1}{(N_c^2 - 1)^2} \langle \text{Tr}[U_{\mathbf{x}_1} U_{\mathbf{x}_2}^\dagger] \text{Tr}[U_{\mathbf{x}_3} U_{\mathbf{x}_4}^\dagger] \rangle = (e^M)_{11} \quad (\text{A5})$$

where the 7×7 matrix M is defined by its elements,

$$M_{ij} = \langle P_i | \hat{M} | P_j \rangle. \quad (\text{A6})$$

All one has to do now is to find the matrix M from Eq. (A6), exponentiate it, picking up the “11” matrix element of the exponential. Such a calculation, while straightforward, is rather involved: here we will utilize the large- N_c limit to construct an approximate result.

Calculating some of the elements of the matrix M and evaluating the N_c -order of the remaining matrix elements yields

$$M = \begin{pmatrix} D_1 & 0 & 0 & 0 & \frac{D_3 - D_2}{\sqrt{N_c^2 - 1}} & 0 & 0 \\ 0 & \frac{1}{2}D_1 + \frac{1}{4}(D_2 + D_3) & O(1/N_c) & O(1/N_c) & \frac{1}{4}(D_3 - D_2) & O(1/N_c) & O(1/N_c) \\ 0 & O(1/N_c) & \dots & \dots & O(1/N_c) & \dots & \dots \\ 0 & O(1/N_c) & \dots & \dots & O(1/N_c) & \dots & \dots \\ \frac{D_3 - D_2}{\sqrt{N_c^2 - 1}} & \frac{1}{4}(D_3 - D_2) & O(1/N_c) & O(1/N_c) & \frac{1}{2}D_1 + \frac{1}{4}(D_2 + D_3) & O(1/N_c) & O(1/N_c) \\ 0 & O(1/N_c) & \dots & \dots & O(1/N_c) & \dots & \dots \\ 0 & O(1/N_c) & \dots & \dots & O(1/N_c) & \dots & \dots \end{pmatrix} \quad (\text{A7})$$

with D_i defined in Eqs. (43) and ellipsis denoting the matrix elements we do not need to calculate as they are at most order-1 in N_c counting. From Eq. (A7) we see that if we start in the color-singlet state $|P_1\rangle$ for the top (bottom) gluon pair, a single interaction can either leave the two gluons in the color-singlet state, or can flip them into a color-octet state $|P_5\rangle$. The latter transition comes in with an order- $1/N_c$ suppression factor. In order to evaluate (A1) we have to start and finish with a color-singlet state: to order- $1/N_c^2$ we may have at most two such transitions: $|P_1\rangle \rightarrow |P_5\rangle$ and the inverse, $|P_5\rangle \rightarrow |P_1\rangle$. Once the system is in the color-octet $|P_5\rangle$ state, it can continue its random walk through color space: however, if we want to keep the calculation at the order- $1/N_c^2$, the interactions between the two transitions should be leading-order in N_c . This is why only the leading- N_c -order matrix elements M_{22} , $M_{25} = M_{52}$, and M_{55} contribute in the 6×6 matrix M_{ij} with $i, j = 2, \dots, 7$: we do not need to calculate the $1/N_c$ -suppressed elements in Eq. (A7) or the elements denoted by ellipsis which can not contribute.

Exponentiating the matrix M from Eq. (A7), picking up the “11” element of the obtained matrix and expanding the result to order- $1/N_c^2$ yields

$$\begin{aligned} \frac{1}{(N_c^2 - 1)^2} \langle \text{Tr}[U_{\mathbf{x}_1} U_{\mathbf{x}_2}^\dagger] \text{Tr}[U_{\mathbf{x}_3} U_{\mathbf{x}_4}^\dagger] \rangle &= e^{D_1} + \frac{(D_3 - D_2)^2}{N_c^2} \left[\frac{e^{D_1}}{D_1 - D_2} - \frac{2e^{D_1}}{(D_1 - D_2)^2} + \frac{e^{D_1}}{D_1 - D_3} - \frac{2e^{D_1}}{(D_1 - D_3)^2} \right. \\ &\quad \left. + \frac{2e^{\frac{1}{2}(D_1 + D_2)}}{(D_1 - D_2)^2} + \frac{2e^{\frac{1}{2}(D_1 + D_3)}}{(D_1 - D_3)^2} \right] + O\left(\frac{1}{N_c^4}\right). \end{aligned} \quad (\text{A8})$$

Finally, noting that (see Eq. (40))

$$\frac{1}{(N_c^2 - 1)^2} \langle \text{Tr}[U_{\mathbf{x}_1} U_{\mathbf{x}_2}^\dagger] \rangle \langle \text{Tr}[U_{\mathbf{x}_3} U_{\mathbf{x}_4}^\dagger] \rangle = e^{D_1} \quad (\text{A9})$$

and using Eq. (41) we obtain Eq. (42).

-
- [1] **STAR** Collaboration, J. Adams *et. al.*, *Distributions of charged hadrons associated with high transverse momentum particles in $p\,p$ and $Au + Au$ collisions at $\sqrt{s(NN)}^{1/2} = 200\text{-GeV}$* , *Phys. Rev. Lett.* **95** (2005) 152301, [[nucl-ex/0501016](#)].
 - [2] **PHENIX** Collaboration, A. Adare *et. al.*, *Dihadron azimuthal correlations in $Au+Au$ collisions at $\sqrt{s_{NN}}=200\text{ GeV}$* , *Phys. Rev.* **C78** (2008) 014901, [[arXiv:0801.4545](#)].
 - [3] **PHOBOS** Collaboration, B. Alver *et. al.*, *High transverse momentum triggered correlations over a large pseudorapidity acceptance in $Au+Au$ collisions at $\sqrt{s_{NN}}=200\text{ GeV}$* , *Phys. Rev. Lett.* **104** (2010) 062301, [[arXiv:0903.2811](#)].
 - [4] **STAR** Collaboration, B. Abelev *et. al.*, *Long range rapidity correlations and jet production in high energy nuclear collisions*, *Phys.Rev.* **C80** (2009) 064912, [[arXiv:0909.0191](#)].
 - [5] **CMS** Collaboration, V. Khachatryan *et. al.*, *Observation of Long-Range Near-Side Angular Correlations in Proton-Proton Collisions at the LHC*, *JHEP* **09** (2010) 091, [[arXiv:1009.4122](#)].
 - [6] **CMS Collaboration**, S. Chatrchyan *et. al.*, *Observation of long-range near-side angular correlations in proton-lead collisions at the LHC*, [arXiv:1210.5482](#).
 - [7] A. Dumitru, F. Gelis, L. McLerran, and R. Venugopalan, *Glasma flux tubes and the near side ridge phenomenon at RHIC*, *Nucl. Phys.* **A810** (2008) 91–108, [[arXiv:0804.3858](#)].
 - [8] S. Gavin, L. McLerran, and G. Moschelli, *Long Range Correlations and the Soft Ridge in Relativistic Nuclear Collisions*, *Phys. Rev.* **C79** (2009) 051902, [[arXiv:0806.4718](#)].
 - [9] N. Armesto, L. McLerran, and C. Pajares, *Long Range Forward-Backward Correlations and the Color Glass Condensate*, *Nucl.Phys.* **A781** (2007) 201–208, [[hep-ph/0607345](#)].
 - [10] N. Armesto, M. Braun, and C. Pajares, *On the long-range correlations in hadron-nucleus collisions*, *Phys.Rev.* **C75** (2007) 054902, [[hep-ph/0702216](#)].
 - [11] K. Dusling, F. Gelis, T. Lappi, and R. Venugopalan, *Long range two-particle rapidity correlations in $A+A$ collisions from high energy QCD evolution*, *Nucl. Phys.* **A836** (2010) 159–182, [[arXiv:0911.2720](#)].
 - [12] A. Dumitru, K. Dusling, F. Gelis, J. Jalilian-Marian, T. Lappi, *et. al.*, *The Ridge in proton-proton collisions at the LHC*, *Phys.Lett.* **B697** (2011) 21–25, [[arXiv:1009.5295](#)].
 - [13] A. Dumitru and J. Jalilian-Marian, *Two-particle correlations in high energy collisions and the gluon four-point function*, *Phys. Rev.* **D81** (2010) 094015, [[arXiv:1001.4820](#)].
 - [14] A. Kovner and M. Lublinsky, *Angular Correlations in Gluon Production at High Energy*, *Phys.Rev.* **D83** (2011) 034017, [[arXiv:1012.3398](#)].
 - [15] F. Gelis, T. Lappi, and R. Venugopalan, *High energy factorization in nucleus-nucleus collisions. 3. Long range rapidity correlations*, *Phys.Rev.* **D79** (2009) 094017, [[arXiv:0810.4829](#)].
 - [16] J. Jalilian-Marian and Y. V. Kovchegov, *Saturation physics and deuteron gold collisions at RHIC*, *Prog. Part. Nucl. Phys.* **56** (2006) 104–231, [[hep-ph/0505052](#)].
 - [17] H. Weigert, *Evolution at small x_{bj} : The Color Glass Condensate*, *Prog. Part. Nucl. Phys.* **55** (2005) 461–565, [[hep-ph/0501087](#)].
 - [18] E. Iancu and R. Venugopalan, *The color glass condensate and high energy scattering in QCD*, [hep-ph/0303204](#).
 - [19] F. Gelis, E. Iancu, J. Jalilian-Marian, and R. Venugopalan, *The Color Glass Condensate*, *Ann.Rev.Nucl.Part.Sci.* **60** (2010) 463–489, [[arXiv:1002.0333](#)].
 - [20] Y. V. Kovchegov and E. Levin, *Quantum Chromodynamics at High Energy*. Cambridge University Press, 2012.
 - [21] L. D. McLerran and R. Venugopalan, *Green’s functions in the color field of a large nucleus*, *Phys. Rev.* **D50** (1994) 2225–2233, [[hep-ph/9402335](#)].
 - [22] L. D. McLerran and R. Venugopalan, *Gluon distribution functions for very large nuclei at small transverse momentum*, *Phys. Rev.* **D49** (1994) 3352–3355, [[hep-ph/9311205](#)].
 - [23] L. D. McLerran and R. Venugopalan, *Computing quark and gluon distribution functions for very large nuclei*, *Phys. Rev.* **D49** (1994) 2233–2241, [[hep-ph/9309289](#)].
 - [24] A. Kovner, L. D. McLerran, and H. Weigert, *Gluon production from nonAbelian Weizsacker-Williams fields in nucleus-nucleus collisions*, *Phys. Rev.* **D52** (1995) 6231–6237, [[hep-ph/9502289](#)].
 - [25] Y. V. Kovchegov and D. H. Rischke, *Classical gluon radiation in ultrarelativistic nucleus nucleus collisions*, *Phys. Rev.* **C56** (1997) 1084–1094, [[hep-ph/9704201](#)].
 - [26] A. Krasnitz, Y. Nara, and R. Venugopalan, *Classical gluodynamics of high energy nuclear collisions: An erratum and an update*, *Nucl. Phys.* **A727** (2003) 427–436, [[hep-ph/0305112](#)].
 - [27] J. P. Blaizot, T. Lappi, and Y. Mehtar-Tani, *On the gluon spectrum in the glasma*, *Nucl. Phys.* **A846** (2010) 63–82, [[arXiv:1005.0955](#)].
 - [28] Y. V. Kovchegov, E. Levin, and L. D. McLerran, *Large scale rapidity correlations in heavy ion collisions*, *Phys. Rev.* **C63** (2001) 024903, [[hep-ph/9912367](#)].
 - [29] I. Balitsky, *Operator expansion for high-energy scattering*, *Nucl. Phys.* **B463** (1996) 99–160, [[hep-ph/9509348](#)].
 - [30] I. Balitsky, *Factorization and high-energy effective action*, *Phys. Rev.* **D60** (1999) 014020, [[hep-ph/9812311](#)].
 - [31] Y. V. Kovchegov, *Small- x F_2 structure function of a nucleus including multiple pomeron exchanges*, *Phys. Rev.* **D60**

- (1999) 034008, [[hep-ph/9901281](#)].
- [32] Y. V. Kovchegov, *Unitarization of the BFKL pomeron on a nucleus*, *Phys. Rev.* **D61** (2000) 074018, [[hep-ph/9905214](#)].
- [33] J. Jalilian-Marian, A. Kovner, and H. Weigert, *The Wilson renormalization group for low x physics: Gluon evolution at finite parton density*, *Phys. Rev.* **D59** (1998) 014015, [[hep-ph/9709432](#)].
- [34] J. Jalilian-Marian, A. Kovner, A. Leonidov, and H. Weigert, *The Wilson renormalization group for low x physics: Towards the high density regime*, *Phys. Rev.* **D59** (1998) 014014, [[hep-ph/9706377](#)].
- [35] E. Iancu, A. Leonidov, and L. D. McLerran, *The renormalization group equation for the color glass condensate*, *Phys. Lett.* **B510** (2001) 133–144.
- [36] E. Iancu, A. Leonidov, and L. D. McLerran, *Nonlinear gluon evolution in the color glass condensate. I*, *Nucl. Phys.* **A692** (2001) 583–645, [[hep-ph/0011241](#)].
- [37] J. L. Albacete and A. Dumitru, *A model for gluon production in heavy-ion collisions at the LHC with rcBK unintegrated gluon densities*, [arXiv:1011.5161](#).
- [38] A. Kovner and M. Lublinsky, *On Angular Correlations and High Energy Evolution*, *Phys. Rev.* **D84** (2011) 094011, [[arXiv:1109.0347](#)].
- [39] E. Levin and A. H. Rezaeian, *The Ridge from the BFKL evolution and beyond*, *Phys. Rev.* **D84** (2011) 034031, [[arXiv:1105.3275](#)].
- [40] A. Kovner and M. Lublinsky, *Angular and long range rapidity correlations in particle production at high energy*, [arXiv:1211.1928](#).
- [41] K. Dusling and R. Venugopalan, *Azimuthal collimation of long range rapidity correlations by strong color fields in high multiplicity hadron-hadron collisions*, *Phys. Rev. Lett.* **108** (2012) 262001, [[arXiv:1201.2658](#)].
- [42] K. Dusling and R. Venugopalan, *Explanation of systematics of CMS p + Pb high multiplicity di-hadron data at $\sqrt{s_{NN}} = 5.02$ TeV*, [arXiv:1211.3701](#).
- [43] K. Dusling and R. Venugopalan, *Evidence for BFKL and saturation dynamics from di-hadron spectra at the LHC*, [arXiv:1210.3890](#).
- [44] E. Gardi, J. Kuokkanen, K. Rummukainen, and H. Weigert, *Running coupling and power corrections in nonlinear evolution at the high-energy limit*, *Nucl. Phys.* **A784** (2007) 282–340, [[hep-ph/0609087](#)].
- [45] Y. Kovchegov and H. Weigert, *Triumvirate of Running Couplings in Small- x Evolution*, *Nucl. Phys.* **A 784** (2007) 188–226, [[hep-ph/0609090](#)].
- [46] I. I. Balitsky, *Quark Contribution to the Small- x Evolution of Color Dipole*, *Phys. Rev. D* **75** (2007) 014001, [[hep-ph/0609105](#)].
- [47] A. Krasnitz and R. Venugopalan, *The initial energy density of gluons produced in very high energy nuclear collisions*, *Phys. Rev. Lett.* **84** (2000) 4309–4312, [[hep-ph/9909203](#)].
- [48] T. Lappi, *Production of gluons in the classical field model for heavy ion collisions*, *Phys. Rev.* **C67** (2003) 054903, [[hep-ph/0303076](#)].
- [49] Y. V. Kovchegov, *Non-Abelian Weizsaecker-Williams field and a two-dimensional effective color charge density for a very large nucleus*, *Phys. Rev.* **D54** (1996) 5463–5469, [[hep-ph/9605446](#)].
- [50] Y. V. Kovchegov, *Quantum structure of the non-Abelian Weizsaecker-Williams field for a very large nucleus*, *Phys. Rev.* **D55** (1997) 5445–5455, [[hep-ph/9701229](#)].
- [51] R. Hanbury Brown and R. Twiss, *A Test of a new type of stellar interferometer on Sirius*, *Nature* **178** (1956) 1046–1048.
- [52] K. Eggert, H. Frenzel, W. Thome, B. Betev, P. Darriulat, et. al., *Angular Correlations Between the Charged Particles Produced in pp Collisions at ISR Energies*, *Nucl. Phys.* **B86** (1975) 201.
- [53] A. H. Mueller, *Small x Behavior and Parton Saturation: A QCD Model*, *Nucl. Phys.* **B335** (1990) 115.
- [54] D. Teaney and R. Venugopalan, *Classical computation of elliptic flow at large transverse momentum*, *Phys. Lett.* **B539** (2002) 53–58, [[hep-ph/0203208](#)].
- [55] G. P. Lepage and S. J. Brodsky, *Exclusive processes in perturbative quantum chromodynamics*, *Phys. Rev.* **D22** (1980) 2157.
- [56] S. J. Brodsky, G. P. Lepage, and P. B. Mackenzie, *On the elimination of scale ambiguities in perturbative quantum chromodynamics*, *Phys. Rev.* **D28** (1983) 228.
- [57] A. H. Mueller, *Soft gluons in the infinite momentum wave function and the BFKL pomeron*, *Nucl. Phys.* **B415** (1994) 373–385.
- [58] Y. V. Kovchegov and K. Tuchin, *Inclusive gluon production in dis at high parton density*, *Phys. Rev.* **D65** (2002) 074026, [[hep-ph/0111362](#)].
- [59] Y. V. Kovchegov and A. H. Mueller, *Gluon production in current nucleus and nucleon nucleus collisions in a quasi-classical approximation*, *Nucl. Phys.* **B529** (1998) 451–479, [[hep-ph/9802440](#)].
- [60] B. Z. Kopeliovich, A. V. Tarasov, and A. Schafer, *Bremsstrahlung of a quark propagating through a nucleus*, *Phys. Rev.* **C59** (1999) 1609–1619, [[hep-ph/9808378](#)].
- [61] A. Dumitru and L. D. McLerran, *How protons shatter colored glass*, *Nucl. Phys.* **A700** (2002) 492–508, [[hep-ph/0105268](#)].
- [62] J. P. Blaizot, F. Gelis, and R. Venugopalan, *High energy p A collisions in the color glass condensate approach. I: Gluon production and the Cronin effect*, *Nucl. Phys.* **A743** (2004) 13–56, [[hep-ph/0402256](#)].
- [63] J. Jalilian-Marian and Y. V. Kovchegov, *Inclusive two-gluon and valence quark-gluon production in DIS and p A* , *Phys. Rev.* **D70** (2004) 114017, [[hep-ph/0405266](#)].
- [64] Z. Chen and A. H. Mueller, *The dipole picture of high-energy scattering, the BFKL equation and many gluon compound states*, *Nucl. Phys.* **B451** (1995) 579–604.
- [65] F. Dominguez, A. Mueller, S. Munier, and B.-W. Xiao, *On the small- x evolution of the color quadrupole and the*

- Weizsäcker-Williams gluon distribution*, *Phys.Lett.* **B705** (2011) 106–111, [arXiv:1108.1752].
- [66] A. Dumitru, J. Jalilian-Marian, T. Lappi, B. Schenke, and R. Venugopalan, *Renormalization group evolution of multi-gluon correlators in high energy QCD*, *Phys.Lett.* **B706** (2011) 219–224, [arXiv:1108.4764].
 - [67] E. Iancu and D. Triantafyllopoulos, *Higher-point correlations from the JIMWLK evolution*, *JHEP* **1111** (2011) 105, [arXiv:1109.0302].
 - [68] D. Grumiller and P. Romatschke, *On the collision of two shock waves in AdS(5)*, *JHEP* **0808** (2008) 027, [arXiv:0803.3226].
 - [69] J. L. Albacete, Y. V. Kovchegov, and A. Taliotis, *Modeling Heavy Ion Collisions in AdS/CFT*, *JHEP* **0807** (2008) 100, [arXiv:0805.2927].
 - [70] J. L. Albacete, Y. V. Kovchegov, and A. Taliotis, *Asymmetric Collision of Two Shock Waves in AdS₅*, *JHEP* **0905** (2009) 060, [arXiv:0902.3046].
 - [71] P. M. Chesler and L. G. Yaffe, *Holography and colliding gravitational shock waves in asymptotically AdS₅ spacetime*, *Phys.Rev.Lett.* **106** (2011) 021601, [arXiv:1011.3562].
 - [72] T. Lappi, S. Srednyak, and R. Venugopalan, *Non-perturbative computation of double inclusive gluon production in the Glasma*, *JHEP* **1001** (2010) 066, [arXiv:0911.2068].
 - [73] N. Borghini, P. M. Dinh, and J.-Y. Ollitrault, *A New method for measuring azimuthal distributions in nucleus-nucleus collisions*, *Phys.Rev.* **C63** (2001) 054906, [nucl-th/0007063].
 - [74] N. Borghini, P. M. Dinh, and J.-Y. Ollitrault, *Flow analysis from multiparticle azimuthal correlations*, *Phys.Rev.* **C64** (2001) 054901, [nucl-th/0105040].
 - [75] U. W. Heinz and B. V. Jacak, *Two particle correlations in relativistic heavy ion collisions*, *Ann.Rev.Nucl.Part.Sci.* **49** (1999) 529–579, [nucl-th/9902020].
 - [76] **STAR Collaboration** Collaboration, J. Adams *et. al.*, *Azimuthally sensitive HBT in Au + Au collisions at $s(NN)^{1/2} = 200$ -GeV*, *Phys.Rev.Lett.* **93** (2004) 012301, [nucl-ex/0312009].
 - [77] G. Kopylov and M. Podgoretsky, *Correlations of identical particles emitted by highly excited nuclei*, *Sov.J.Nucl.Phys.* **15** (1972) 219–223.
 - [78] A. Capella, A. Krzywicki, and E. Levin, *Pion interferometry and intermittency in heavy ion collisions*, *Phys.Rev.* **D44** (1991) 704–716.
 - [79] M. Asakawa, T. Csorgo, and M. Gyulassy, *Squeezed correlations and spectra for mass shifted bosons*, *Phys.Rev.Lett.* **83** (1999) 4013–4016, [nucl-th/9810034].
 - [80] T. Csorgo and S. S. Padula, *Disappearance of Squeezed Back-to-Back Correlations: A New signal of hadron freeze-out from a supercooled Quark Gluon Plasma*, *Braz.J.Phys.* **37** (2007) 949–962, [arXiv:0706.4325].
 - [81] Y. V. Kovchegov and K. L. Tuchin, *Elliptic flow from minijet production in heavy ion collisions*, *Nucl.Phys.* **A708** (2002) 413–434, [hep-ph/0203213].
 - [82] Y. V. Kovchegov and K. L. Tuchin, *Correlation functions and cumulants in elliptic flow analysis*, *Nucl.Phys.* **A717** (2003) 249–267, [nucl-th/0207037].
 - [83] **ALICE Collaboration** Collaboration, B. Abelev *et. al.*, *Long-range angular correlations on the near and away side in p-Pb collisions at $\sqrt{s_{NN}} = 5.02$ TeV*, arXiv:1212.2001.
 - [84] Y. V. Kovchegov, *Diffraction gluon production in proton nucleus collisions and in DIS*, *Phys. Rev.* **D64** (2001) 114016, [hep-ph/0107256].
 - [85] C. Marquet and H. Weigert, *New observables to test the Color Glass Condensate beyond the large- N_c limit*, *Nucl. Phys.* **A843** (2010) 68–97, [arXiv:1003.0813].
 - [86] N. Nikolaev, W. Schafer, and B. Zakharov, *Nonlinear $k(\text{perpendicular})$ -factorization for gluon-gluon dijets produced off nuclear targets*, *Phys.Rev.* **D72** (2005) 114018, [hep-ph/0508310].
 - [87] P. Cvitanovic, *Group theory: Birdtracks, Lie's and exceptional groups*. 2008. Available online at <http://birdtracks.eu/>.